ACCSCIENCE PUBLISHING

International Journal of Bioprinting

RESEARCH ARTICLE

Sericin improves alginate-gelatin hydrogels' mechanical properties, porosity, durability, and viability of fibroblasts in cardiac spheroids

Martine Tarsitano[1,2], Clara Liu Chung Ming[1,3], Dana Idais[1,3], Hadi Mahmodi[4], Kaitlin Wyllie[5,6], Benedetta Isella[7], Thomas R. Cox[5,6], Irina Kabakova[4], Donatella Paolino[2,8], and Carmine Gentile[1,3]*

[1]School of Biomedical Engineering, Faculty of Engineering and IT, University of Technology Sydney, Ultimo, Sydney, NSW, Australia

[2]Department of Experimental and Clinical Medicine, School of Medicine and Surgery, University "Magna Graecia" of Catanzaro, Catanzaro, Italy

[3] Heart Research Institute, Newtown, Sydney, NSW, Australia

[4]School of Mathematical and Physical Sciences, Faculty of Science, University of Technology Sydney, Ultimo, NSW, Australia

[5]The Garvan Institute of Medical Research and The Kinghorn Cancer Centre, Darlinghurst, NSW, Australia

[6]School of Clinical Medicine, St Vincent's Healthcare Clinical Campus, UNSW Medicine and Health, Sydney, NSW, Australia

[7] Fibrothelium GmbH, Philipsstraße 8, Aachen, Germany

[8]Research Center "ProHealth Translational Hub", Department of Experimental and Clinical Medicine, "Magna Graecia" University of Catanzaro, Catanzaro, Italy

(This article belongs to the Special Issue: *3D Bioprinting DownUnder: Innovation, Advancements and Perspectives*)

***Corresponding author:**
Carmine Gentile
(carmine.gentile@uts.edu.au)

Citation: Tarsitano M, Ming CLC, Idais D, et al. Sericin improves alginate-gelatin hydrogels' mechanical properties, porosity, durability, and viability of fibroblasts in cardiac spheroids. *Int J Bioprint*. 2024. doi: 10.36922/ijb.5678

Received: October 29, 2024
Revised: November 21, 2024
Accepted: November 26, 2024
Published Online: November 27, 2024

Abstract

Biofabrication of cardiac patches is a challenging strategy proposed as an alternative to transplantation for end-stage heart failure patients. The optimization of the bioink used for this strategy can be limited by costs, properties, and biocompatibility of its building blocks. Lately, sericin has emerged within a wide range of natural proteins, thanks to its bioadhesive and biocompatibility potential. In this study, we assessed for the first time the effects of adding silk sericin on alginate-gelatin hydrogels, proposed for cardiac applications. To this aim, we first biofabricated sericin-containing hydrogels with increasing protein concentrations. Thus, we characterized hydrogels' mechanical behavior, porosity and structure through rheology, Brillouin microspectroscopy, and scanning electron microscopy. Then, we bioprinted the formulated hydrogels and evaluated their effects on human cardiac spheroids (CSs) *in vitro*. Our mechanical characterization demonstrated that adding sericin significantly enhanced the elasticity and the viscosity of alginate-gelatin hydrogels. Sericin also modified hydrogels' swelling behavior and their pore size, increasing by 20%, 62%, and 92% in Ser1%, Ser2%, and Ser3%, respectively. Although Ser1% did not exhibit significant effects on CSs, Ser2% and Ser3% enhanced cardiac cell viability for up to 14 days compared to the sericin-free hydrogel by acting on the fibroblast population. Sericin-based bioinks showed better printability and durability with +33% and +28% intact patches after 28 days of culture at 37°C compared to alginate-gelatin. Taken together, our results validated the use of sericin as a promising component for the optimization of bioink intended for cardiac applications.

Keywords: Sericin; Hydrogels; Cardiac spheroids; Myocardial infarction; Biomaterials; Alginate; Gelatin; 3D bioprinting

1. Introduction

Myocardial infarction (MI) remains a leading cause of morbidity and mortality worldwide.[1] By itself, an adult myocardium has low regenerative capacity compared to other tissues in the human body, especially when myocardial cells have been damaged after MI.[2] Instead of replacing the injured area with functional tissue, the physiological repairing response after MI results in the formation of fibrotic scar tissue, which thickens the heart wall and triggers left ventricular remodeling.[3] These events reduce the mechanical support to the organ, which is deprived of its full functionality to pump blood, due to the increased workload and oxygen demand, contributing to an increased risk of arrhythmias and the development of a failing heart.[4] The permanent remedy for patients with end-stage heart failure (HF) is heart transplantation.[5] However, heart transplantation is restricted by limited donors' availability and is associated with several post-surgery complications, such as graft rejection and immunosuppression-related problems.[5–7] In this scenario, cardiac bioengineering offers advanced and personalized approaches to transform MI treatment through innovative technologies, such as 3D bioprinting, as alternatives to whole-organ transplantation.[8,9] The epicardial application of 3D-bioprinted cardiac patches represents a pivotal technique aimed at repairing myocardial tissue after MI.[10–12] This approach allows to deliver cells with regenerative potential (such as stem cells) directly in the proximity of the injured myocardial area and provides mechanical support for the native myocardium, preventing its further deterioration after MI-related events.[13–16] Moreover, the evolution of the field enabled the possibility to create patient-tailored cardiac patches, by designing their shape and size to match the patient's specific infarcted region.[17] During the design of a cardiac patch, the selection of the bioink represents a fundamental step.[10,12] A suitable bioink should be able to both mimic the native extracellular matrix (ECM) and match mechanical properties standards to support the stress caused by cardiac mechanical forces.[18,19] Hydrogel-based bioinks, particularly those derived from natural polymers, have been widely used as biomaterials for these aims, thanks to their high biocompatibility, tunable mechanical properties, and ability to resemble the ECM organization.[11,20–23] Our team has previously proposed cardiac spheroids (CSs) as bioengineered cardiac tissues able to model the human cardiac pathophysiology *in vitro*.[24–27] We used CSs combined with a natural polymers-derived hydrogel, made of alginate and gelatin, to 3D-bioprint functional cardiac patches, which provided cardiac cells integration and viability *in vitro* and improved myocardial function in an *in vivo* model of MI.[25,28,29] Although these constructs were successfully transplanted during the testing on small animal modes, their mechanical properties, printability, and durability could be further improved to better match the requirements of the human cardiac tissue.[29,30]

Sericin is the globular protein that constitutes 25–30 wt% of the whole silk filament.[31] Sericin has the function of enveloping and binding the fibroin strands together, creating a layer which protects the cocoon from harmful microorganisms, such as bacteria and fungi.[32] The glue-like nature of sericin is crucial to ensure the cocoon's development and the maintenance of its structural integrity.[31] While silk fibroin has been widely used for biomedical applications due to its suitable elasticity, mechanical strength, and tunable degradation, silk sericin has been ignored and discarded as a byproduct of silk production in the textile industry, causing environmental pollution.[33] At present, intrinsic properties of sericin make it a promising candidate for biomedical applications, and its use provides a strong contribution to the "waste to resource" platform.[33,34] Sericin is rich in non-essential amino acids (e.g., serin, aspartic acid, glutamic acid, and glycine) and its intrinsic adhesive nature promotes cell growth and proliferation.[35,36] Compared to silk fibroin, sericin has reduced β-sheets structures, which results in difficult hydrogel formation, and this phenomenon justifies the often blending of sericin with other polymers, such as alginate.[37,38] When non-coupled with fibroin, sericin is low-immunogenic, and its anticancer, antioxidant, anticoagulation, anti-inflammatory, antibacterial, and wound healing properties have been documented in several drug delivery and tissue engineering studies.[39–43] This collected knowledge promises an interesting translation of sericin-based materials into cardiac tissue engineering. Although silk fibroin has been widely investigated in the preparation of both cardiac injectable hydrogels and 3D-bioprinted patches,[44] only a few studies have examined the role of sericin as a building block in biomaterials intended for the treatment of MI.[36,45]

In this study, we propose biofabricated alginate-gelatin hydrogels supplemented with sericin from silkworm (*Bombyx mori*). We hypothesize that, owing to its properties and structure, sericin may improve the mechanical characteristics of alginate-gelatin hydrogels, enhancing their elasticity without affecting the cardiac

cell viability of hydrogel-embedded CSs. The hypothesis was tested by biofabricating alginate-gelatin hydrogels with increasing sericin concentrations, which were first characterized in their mechanical properties by Brillouin microspectroscopy and classic rheology. The swelling and porosity properties were assessed by gravimetric and liquid displacement methods, while scanning electron microscopy (SEM) allowed us to evaluate the inner morphology of the biofabricated hydrogels and measure their pore sizes. All the prepared hydrogels were 3D-bioprinted to assess whether the addition of sericin affects the printability and durability of the biomaterials. Finally, CSs were generated *in vitro* and embedded in sericin-containing hydrogels to evaluate the toxicity ratio and cardiac cell distribution after incubation in the medium for up to 28 days.

2. Materials and methods

2.1. Materials

Alginic acid sodium salt from brown algae, gelatin from bovine skin, sericin *B. mori* (silkworm), calcium chloride, Dulbecco's phosphate-buffered saline (DPBS) with no calcium chloride or magnesium chloride, agarose, L-glutamine solution 200 mM, high-glucose Dulbecco's Modified Eagle's Medium (DMEM), Triton™ X-100, bovine serum albumin, and formalin solution were purchased from Sigma Adrich (Castle Hill, NSW, Australia). PureSilk® Sericin was kindly provided by Fibrothelium GmbH (Aachen, Germany) and used to perform comparative Brillouin microspectroscopy studies only. Penicillin-Streptomycin (Pen/Strep; Gibco) was obtained from Thermo Fisher Scientific Australia (Scoresby, VIC, Australia). Purified mouse anti-human CD31 was purchased from BD Life Sciences (Macquarie Park, NSW, Australia). Secondary donkey anti-mouse antibodies Alexa Fluor® 647-conjugated was purchased from Jackson ImmunoResearch Laboratories Inc. (West Grove, PA, USA). Troponin T-C Antibody (CT3) Alexa Fluor® 546-conjugated (cTNT) was obtained from Santa Cruz Biotechnology Inc. (Heidelberg, Germany). Alexa Fluor® 488 Anti-Vimentin antibody [V9] was purchased from Abcam (Melbourne, VIC, Australia). NucBlue™ Hoechst 33342 and LIVE/DEAD™ Viability/Cytotoxicity Kit (calcein-AM and ethidium homodimer-1) were purchased from Thermo Fisher Scientific Australia (Scoresby, VIC, Australia).

2.2. Preparation of hydrogels

Our previously established protocol was used during the preparation of alginate-gelatin hydrogels.[29,30] Briefly, alginic sodium salt (Alg, 4% w/v), gelatin (Gel, 8% w/v), and sericin (Ser, 0%, 1%, 2%, and 3% w/v) powders were first sterilized under UV light for 30 min. DMEM supplemented with 1% v/v Pen/Strep and 1% v/v L-glutamine 200 mM was heated at 50°C on Heating Plate Cimarec® (ThermoFisher Scientific) and the powders were slowly inserted under continuous stirring in a biosafety cabinet until they were completely solubilized in the media. The achieved hydrogel formulations (named henceforth as Ser0%, Ser1%, Ser2%, and Ser3%) were aliquoted and then sealed. All the aliquots were stored at 4°C for further analysis. The ionic cross-linking was performed with 2% w/v $CaCl_2$ solution promptly sterilized by filtration at 0.2 μm and added on top of gelated hydrogels.[30] Figure 1 provides a schematic representation of the biofabrication of sericin-containing hydrogels and the experimental plan.

2.3. Fourier transform infrared spectroscopy analysis

To identify any interactions occurring among sericin, alginate, and gelatin, a Fourier transform infrared spectroscopy (FTIR) study was carried out using a Nicolet™ iS™5 FT-IR Spectrometer (Thermo Fisher Scientific Inc., Waltham, MA, USA) equipped with an iD7 attenuated total reflectance (ATR) device. The vibrational spectra of single components' powders and freeze-dried crosslinked sericin-containing hydrogels were obtained at room temperature (25°C), using 64 scans and 4 cm^{-1} resolution, within the spectral region from 4000 to 400 cm^{-1} in transmission mode. OMNIC software (version 9.12.1019), Thermo Fisher Scientific, Waltham, MA, USA was used to automatically detect the peaks of the spectra.

2.4. Swelling test

The change in swelling properties of the hydrogels was evaluated by a gravimetric method as previously reported.[46] Briefly, freeze-dried sericin-containing hydrogels were immersed in PBS (pH 7.4) at 37°C. At specific time points (0, 0.5, 1, 2, 4, 6, and 24 h), hydrogels were withdrawn from PBS, wiped off excess buffer, and weighed. The swelling ratio (%) was calculated according to the following equation:

$$\text{Swelling ratio}(\%) = \frac{W_{wet} - W_{dry}}{W_{dry}} \times 100 \quad \text{(I)}$$

where W_{dry} is the weight of the freeze-dried hydrogel before the immersion in PBS, and W_{wet} is the weight of swollen hydrogel recorded at each time point.

2.5. Brillouin microspectroscopy and rheological characterization of hydrogels

Hydrogels were evaluated in their mechanical properties through rheology and Brillouin microspectroscopy. The rheological characterization of hydrogels before crosslinking involved the evaluation of dynamic moduli

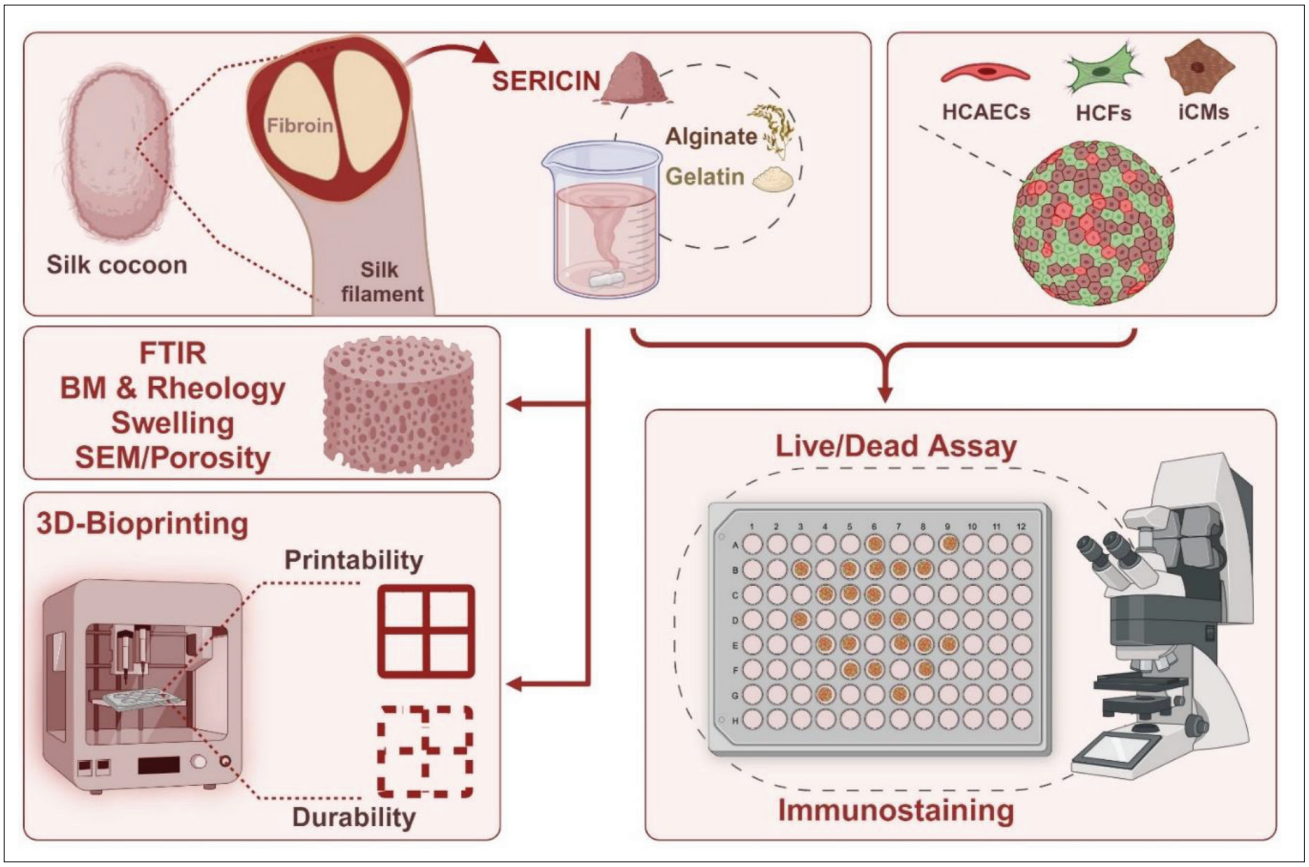

Figure 1. Schematic representation of the experimental plan. Silk sericin was used as an additive component in alginate-gelatin hydrogel biofabrication to obtain sericin-containing hydrogels at 1%, 2%, and 3% w/v sericin concentrations. We carried out FTIR studies on biofabricated hydrogels to assess their secondary structure and confirm the inclusion of sericin within the hydrogel network. Hydrogels were characterized by Brillouin microspectroscopy and rheology to assess their mechanical behavior and by SEM to observe the inner morphology. The gravimetric method on freeze-dried samples assessed the hydrogels' porosity as well as their swelling behaviors. All the biofabricated hydrogels were then 3D-bioprinted to evaluate their resolution after printing and durability after incubation at 37°C in the cell medium. CSs were generated by co-culturing HCAECs, HCFs, and iCMs, thus embedded in the biofabricated hydrogels to assess cardiac cell viability and distribution after 3, 14, and 28 days of incubation. Abbreviations: BM, Brillouin microspectroscopy; CSs, cardiac spheroids; FTIR, Fourier transform infrared spectroscopy; HCAECs, human coronary artery endothelial cells; HCFs, human cardiac fibroblasts; iCMs, iCell® cardiomyocytes; SEM, scanning electron microscopy.

(G', G'', and η^*) during oscillatory frequency sweep testing by using Kinexus® Pro rotational rheometer (Malvern Panalytical Ltd., Worcester, UK) equipped with a cone-plate geometry (diameter 40 mm, angle 2°). Each sample was gently put on lower geometry, previously heated and maintained at 25°C or 28°C by the connected Pelter unit (Malvern Panalytical Ltd., Worcester, UK). The sample was kept at rest for 5 minutes before starting the analysis, to dismiss any effect of sample loading on the rheological evaluation. The gap between geometries was fixed at 1 mm, and the operating frequency range was set at 0.1–10 Hz) with a constant shear stress of 1 Pa.[47] After crosslinking, the hydrogels were characterized by employing a dynamic hybrid rheometer (DHR-3, TA Instruments, New Castle, DE, USA) in an unconfined compression test. Each sample was molded using punch biopsies (8 mm diameter, KAI's Medical Products, Japan) and placed between the upper and lower geometries (8.0 mm parallel plate, Peltier plate Stainless steel, TA Instruments, New Castle, DE, United States). The unconfined compression test was performed at 25°C with a constant compression rate of 2 μm/s, by recording the axial force (N) and gap (μm) values as output data. The collected data were processed to obtain a stress–strain curve, and Young's modulus (kPa) was obtained from the linear region of the curve.[29]

Brillouin microspectroscopy apparatus involved a laser with approximately 200 mW continuous wave emission at 660 nm wavelength (Torus, Laser Quantum, Stockport, United Kingdom), integrated with a confocal microscope (CM1, The Table Stable Ltd., Mettmenstetten, Switzerland), a 3D scanning microscopy stage (SmarAct, Oldenburg, Germany), and a 6-pass scanning tandem Fabry-Perot interferometer (TFP1, The Table Stable Ltd.,

Mettmenstetten, Switzerland). This system was used to collect the spontaneous Brillouin scattering spectra, where the backscattered light was collected by an objective lens (20× Mitutoyo Plan Apo infinity corrected objective, NA = 0.42, WD = 20 mm) and subsequently redirected to the interferometer for analysis. The analysis was carried out on hydrogels before and after crosslinking and after incubation in DMEM (in the incubator at 37°C, 5% CO_2) to avoid hydrogel dehydration. Each sample was analyzed by recording the raw spectra of Stokes and Anti-Stokes Brillouin peaks at four arbitrary points within each hydrogel sample. The collected raw data were analyzed by fitting a Lorentzian model to every Stokes and Anti-Stokes Brillouin peak, produced as a result of optoacoustic interaction within the gel. The line fit was performed using Ghost Software ver. 7.00 (The Table Stable Ltd., Mettmenstetten, Switzerland) and the average value between Stokes and Anti-Stokes peaks was taken as the final Brillouin frequency shift (BFS; GHz, directly related to elasticity) or Brillouin linewidth (BLW; GHz, directly related to viscosity) to eliminate the influence of possible laser frequency drifting during the experiment. The hydrogels were analyzed before crosslinking, after crosslinking, and after incubation in DMEM (in an incubator at 37°C, 5% CO_2).[48]

2.6. Determination of pore size and porosity

The inner morphology of hydrogels was evaluated by means of SEM. The hydrogels (1 mL) were cast in 6-well plates and crosslinked after gelation. Squared cross-sections were cut from the center of each well to ensure a uniform surface, subsequently mounted on stubs covered with double adhesive carbon tabs and fully dried in a vacuum oven (100 kPa, Gallenkamp OVA031.XX1.5, Manchester, United Kingdom) for 24 h. Hereafter, a sputter coater machine (Leica EM ACE600, Leica Microsystems Pty Ltd, Macquarie Park, NSW, Australia) was employed to perform a 10 nm gold coating of samples, which were then imaged using the Zeiss EVO LS15 scanning electron microscope (Zeiss, Macquarie Park, NSW, Australia), furnished with a thermionic tungsten electron gun, by setting an acceleration voltage of 10 kV and a working distance of 10.5 mm. At least 15 images from random areas were acquired for each sample by Zeiss SmartSEM software and analyzed for pore size (area, μm^2) using ImageJ software by manually marking the perimeter borders of every single pore and using the measure tool of the software (Figure S1, Supporting Information), as previously reported.[29,49–51] The porosity of the biofabricated hydrogels was determined by the liquid displacement method as previously reported.[52,53] In detail, the freeze-dried hydrogels were submerged in a known volume (V_1) of PBS (pH 7.4) within a 10 mL graduated cylinder. After 2 h, the total volume was recorded (V_2), the swollen hydrogel removed, and the remaining liquid volume inside the cylinder was recorded (V_3). The porosity (%) was calculated according to the following equation:

$$\text{Porosity}(\%) = \frac{V_1 - V_3}{V_2 - V_3} \times 100 \quad \text{(II)}$$

2.7. 3D bioprinting, printability, and durability assessments

Sericin-containing hydrogels were 3D-bioprinted using the extrusion-based bioprinter BIO X6 (CELLINK, Gothenburg, Sweden) in simple squares with an internal cross to evaluate their printability and durability. The bioprinter chamber was sterilized with UV light and all the pre-printing stages were performed in a biosafety cabinet to ensure sterility conditions. At the moment of bioprinting, each hydrogel was warmed up to 30°C in a water bath and then transferred into a 3 mL cartridge by using a luer lock syringe and connector to avoid the formation of bubbles. The cartridge was then mounted with a 22G nozzle, with an inner diameter of 0.41 mm, and moved into a temperature-controlled printhead (with a control precision within 0.5 °C). The 3D model consisted of a 16 × 16 × 0.41 mm^3 (width × length × height) patch printed with two consecutive layers, and it was generated with DNA Studio 4 Software equipped with G-code Editor (CELLINK, Gothenburg, Sweden). To maintain the hydrogel in liquid state and allow rapid gelation during and after the printing, the printhead and the printbed temperatures were set at 28 and 10 °C, respectively. The printability of the bioprinted patches (n = 14) was assessed before crosslinking by measuring the inner width of the gelated hydrogel strands with ImageJ[50] and then comparing the value with the inner diameter of the nozzle according to the following equation:

$$\text{Printability ratio}(\text{AU}) = \frac{W_{pf}}{D_n} \quad \text{(III)}$$

where W_{pf} represents the width of the printed strand, and D_n is the inner diameter of the 22G nozzle.

The obtained 3D models were crosslinked with $CaCl_2$ solution and afterwards, they were submerged with DMEM and incubated (37°C, 5% CO_2 in air) for up to 28 days. The medium was withdrawn and replaced with fresh DMEM every 4 days, minimizing the movement during the procedure. To assess their durability in the cell culture medium, the patches were monitored for macroscopic disintegration by imaging them with EVOS

M7000 Imaging System (Thermo Fisher Scientific Inc., Scoresby, VIC, Australia) at fixed time points from the day of printing (day 0) and after 1, 3, 7, 14, 21, and 28 days of incubation. When any sign of the disintegration of the main structure occurred (such as dissolving or detachment of small hydrogel's fragments), the patch was considered "non survival."[30]

2.8. Cell culture and CS generation

Human cardiac fibroblasts (HCFs) and human coronary artery endothelial cells (HCAECs) were obtained from Cell Applications (San Diego, CA, USA), and they were cultured in Human Cardiac Fibroblast medium and MesoEndo growth medium (Cell Applications, Inc, San Diego, CA, USA), respectively. iCell® Cardiomyocytes (iCMs, cardiomyocytes differentiated from human-induced pluripotent stem cells) were obtained from FujiFilm Cellular Dynamics (Madison, WI, USA). According to the provider's instructions, iCMs were plated in iCell® Plating Medium and cultured in iCell® Maintenance Medium (Fujifilm Cellular Dynamics, Inc., Madison, WI, USA). The generation of human CSs was achieved by co-culturing HCFs, HCAECs, and iCMs at a ratio of 1:1:2, as reported in previous studies.[24,26,29] Non-adherent agarose microwells were formed by using 12–81 3D Petri Dish® cast silicone molds (Microtissues Inc., Providence RI, USA). Briefly, the autoclaved molds were filled with molten agarose (2% w/v in DPBS), once cooled at room temperature, the microwells were taken out from the mold and moved to 12-well plates submerged in DMEM and left in the incubator (37°C, 5% CO_2 in air) for 2 days to equilibrate while the medium was frequently refreshed. At the moment of CS generation, each cell type was spun and then combined by resuspending the pellets in CS medium (HCF medium, MesoEndo growth medium and iCell® maintenance medium at a 1:1:2 ratio).[26,29] The cellular suspension was seeded in the pre-equilibrated microwell chamber, and the constructs containing cells were incubated again. After a few hours, the cells started spontaneously to aggregate in the microwells, generating 81 CSs/agarose structure. The CS medium was refreshed until CSs were formed. For *in vitro* studies and imaging the CSs ($n \geq 3$) were plated in glass-bottom 96-well plates (Miltenyi Biotec, Macquarie Park, NSW, Australia) and the warm hydrogel (100 µL, 37°C) was added on top.[24]

2.9. Contractile activity and optical mapping measurements

To measure the contraction frequency (number of CS contractions per second) and the fractional shortening % (FS%), we recorded videos of contracting CSs in Ser0% and Ser3% hydrogels using the EVOS M7000 Imaging System (Thermo Fisher Scientific Inc., Scoresby, VIC, Australia) after 3, 14, and 28 days of incubation in normoxic conditions (37°C, 5% CO_2), as previously described.[54] To measure the conduction velocity (CV), CSs were plated in an 8-well chamber and incubated for 14 days at 37°C, 5% CO_2. CS-containing wells were loaded with 17.7 µM Rhod-2 AM (fluorescent Ca^{2+} indicator, Abcam, Melbourne, VIC, Australia), 0.02% Pluronic™ F127 (Thermo Fisher Scientific Inc., Scoresby, VIC, Australia), and 50 µM RH237 (Santa Cruz Biotechnology Inc., Heidelberg, Germany), and incubated for 2 h at 37°C, 5% CO_2. Each well was then washed with fresh culture medium three times and incubated for an additional 30 min with media prior to the individual transfer of CSs to 60 mm sterile cell culture plates (Corning). When ready for imaging, CSs were carefully moved to the OMS-PCIE-2002 optical mapping chamber (Mapping Lab Ltd, Manchester, UK) under an upright microscope equipped with high-speed CMOS cameras. Briefly, RH237 fluorescence as a function of the action potential was passed through a long-pass dichroic filter of 700 nm (FELH700, Thorlabs, Newton, NJ, USA), while Rhod-2 AM fluorescence as a function of Ca^{2+} was passed through a long-pass dichroic filter of 585 nm (FBH585, Thorlabs, Newton, NJ, USA). Both fluorescence signals were collected through a long-pass dichroic beamsplitter with a cutoff wavelength of 638 nm (DMLP638, Thorlabs, Newton, NJ, USA), then filtered by a 550 nm long-pass filter (FELH550, Thorlabs, Newton, NJ, USA) before voltage signals were imaged. A spatial resolution maximum of 512 × 512 pixels was utilized during acquisition, with a total mapping area of 64 × 64. Temporal resolution was set to 1000 frames/second at an exposure time of 0.9 ms over 10 s of recording time. Data were acquired in real-time using an 8-channel TTL analog-digital converter and OMapRecord 4.0 software (Mapping Lab Ltd, Manchester, UK), then processed using OMapScope 5.6.8 (Mapping Lab Ltd, Manchester, UK). Processing filters were applied to generate waveforms with low noise-to-signal ratios including a Gauss convolution of 9 × 9, a zero-phase filter window of 30, and theta smoothing intensity of 1.5. Waveform graphs were selected based on a selected region of interest (ROI) to display the lowest signal-to-noise ratio. A single peak representing a single contraction was used for calculating the CV values for action potential and calcium signals, per array, including temporal sequence recordings (slowed to 1/20th of the original speed) to display the propagation of signals at different regions of the CSs.

2.10. Live/Dead staining and immunostaining of CSs

To assess the cell viability of CSs embedded in sericin-containing hydrogels, the dead/live cells ratio was estimated over time at fixed time points, as previously described.[29,30] Briefly, CSs embedded in hydrogels were cultured in the incubator (37°C, 5% CO_2) for up to 28 days, by replacing the

medium every 2 days, and the viability was evaluated after 3, 14, and 28 days. LIVE/DEAD™ Viability/Cytotoxicity Kit and NucBlue™ were used to detect living cells, dead and total cells, by staining them with calcein-AM (1 µL/mL), ethidium homodimer-1 (EthD-1, 1 µL/mL), and Hoechst stain, respectively. The dyes were directly added to the medium on top of CSs-containing hydrogels and then incubated at 37°C (5% CO_2) for 3 h. After the incubation, the samples were washed three times with warm DPBS, according to the manufacturer's directions, and finally imaged with a STELLARIS 8 confocal microscope (Leica Microsystems Pty Ltd, Macquarie Park, NSW, Australia).

After 28 days of incubation, all cell types present in CSs embedded in hydrogels were identified by immunostaining. The samples were first fixed in 4% paraformaldehyde for 3 h at room temperature, washed in PBSA 0.01% (DPBS containing 0.01% sodium azide), permeabilized in 0.02% Triton-X/PBSA for 1 h, blocked with 3% BSA/PBSA, and then incubated with suitable primary and secondary antibodies at 4°C for 18 h.[26] HCAECs were labeled by primary mouse anti-human CD31 (6.25 µg/mL), revealed by a secondary donkey anti-mouse Alexa Fluor® 647-conjugated antibody (21 µg/mL). Troponin T-C Antibody (CT3) Alexa Fluor® 546-conjugated (10 µg/mL), Alexa Fluor® 488 Anti-Vimentin antibodies (2 µg/mL), and NucBlue™ (2 drops/mL) were used to stain iCMs, HCFs, and nuclei, respectively. All samples were imaged by STELLARIS 8 confocal microscope and the collected images were processed in ImageJ and Adobe Photoshop 25.3.1 (Adobe Systems, Inc., San Jose, CA, USA).[50] 3D-rendered images and videos were produced using Imaris visualization software (Oxford Instruments, Abingdon, Oxfordshire, UK).[28]

2.11. Statistical analysis

All the collected data were analyzed and plotted using GraphPad Prism version 8.4.2 for Windows (GraphPad Software, Boston, MA, USA). Swelling test results were analyzed using two-way analysis of variance (ANOVA) with Dunnett's multiple comparisons test. For all other experiments, we employed Brown–Forsythe and Welch ANOVA followed by Dunnett's multiple comparisons test. All results are expressed as mean ± standard error of mean (SE).

3. Results and discussion

3.1. The inclusion of sericin modulates the mechanical properties of alginate-gelatin hydrogels

To biofabricate sericin-containing alginate-gelatin hydrogels, we chose a range of sericin concentrations (1, 2, and 3% w/v) based on previous studies, which investigated the role of this protein in the formulation of functional hydrogels and scaffolds for biomedical purposes.[36,37,55] To characterize hydrogels' secondary structures, we first performed FTIR analyses on both freeze-dried hydrogels and single-component dry powders (Figure 2). Figure 2A shows the FTIR spectra of pure alginate, gelatin, and

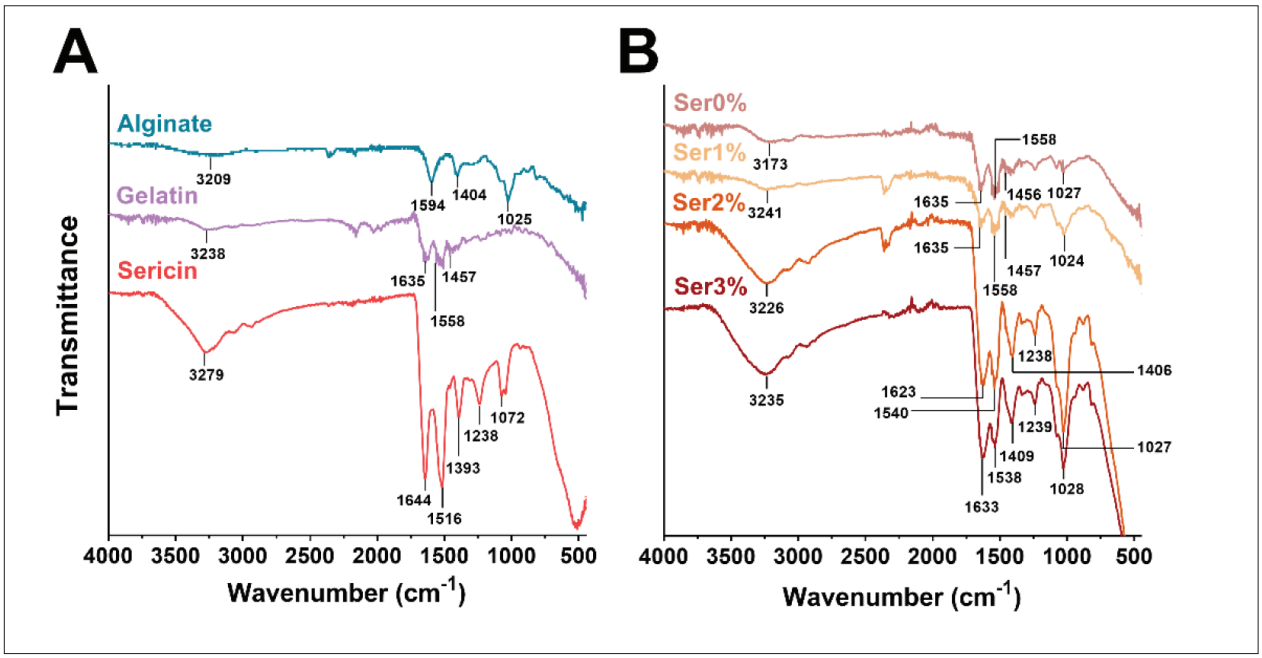

Figure 2. Secondary structure investigation by FTIR spectroscopy of sericin-containing alginate-gelatin hydrogels and their main components. FTIR spectra of alginate, gelatin, and sericin dry powders (A) and sericin-containing hydrogels freeze-dried after crosslinking (B). Abbreviation: FTIR, Fourier transform infrared spectroscopy.

sericin powders used in this study. The all components, in dry powder form, exhibited a broad peak at ~3200 cm^{-1} (hydroxyl group), related attributed to O—H stretching vibration, which was more pronounced in sericin's spectra due to the high content of serine amino acid.[56,57] The spectrum of alginic acid powder exhibits the typical peaks of the asymmetric and symmetric carboxyl group (—COOH stretching) of the polymeric backbone at 1594 and 1404 cm^{-1}, respectively.[58] In gelatin and sericin spectra, we identified peaks at 1635 and 1644 cm^{-1} (amide I), 1516 and 1558 cm^{-1} (amide II), and 1238 cm^{-1} (amide III), which were related to C=O stretching, N–H bending, and C–N stretching vibrations, respectively. All these peaks, together with sericin's footprint are visible in the spectra derived from all sericin-containing hydrogels (Figure 2B), confirming the incorporation of the silk protein within the polymeric network. Next, to evaluate the mechanical properties of the biofabricated hydrogels containing sericin, we performed a mechanical characterization through Brillouin microspectroscopy and classic rheology analyses. These methodologies provided complementary information on hydrogels'

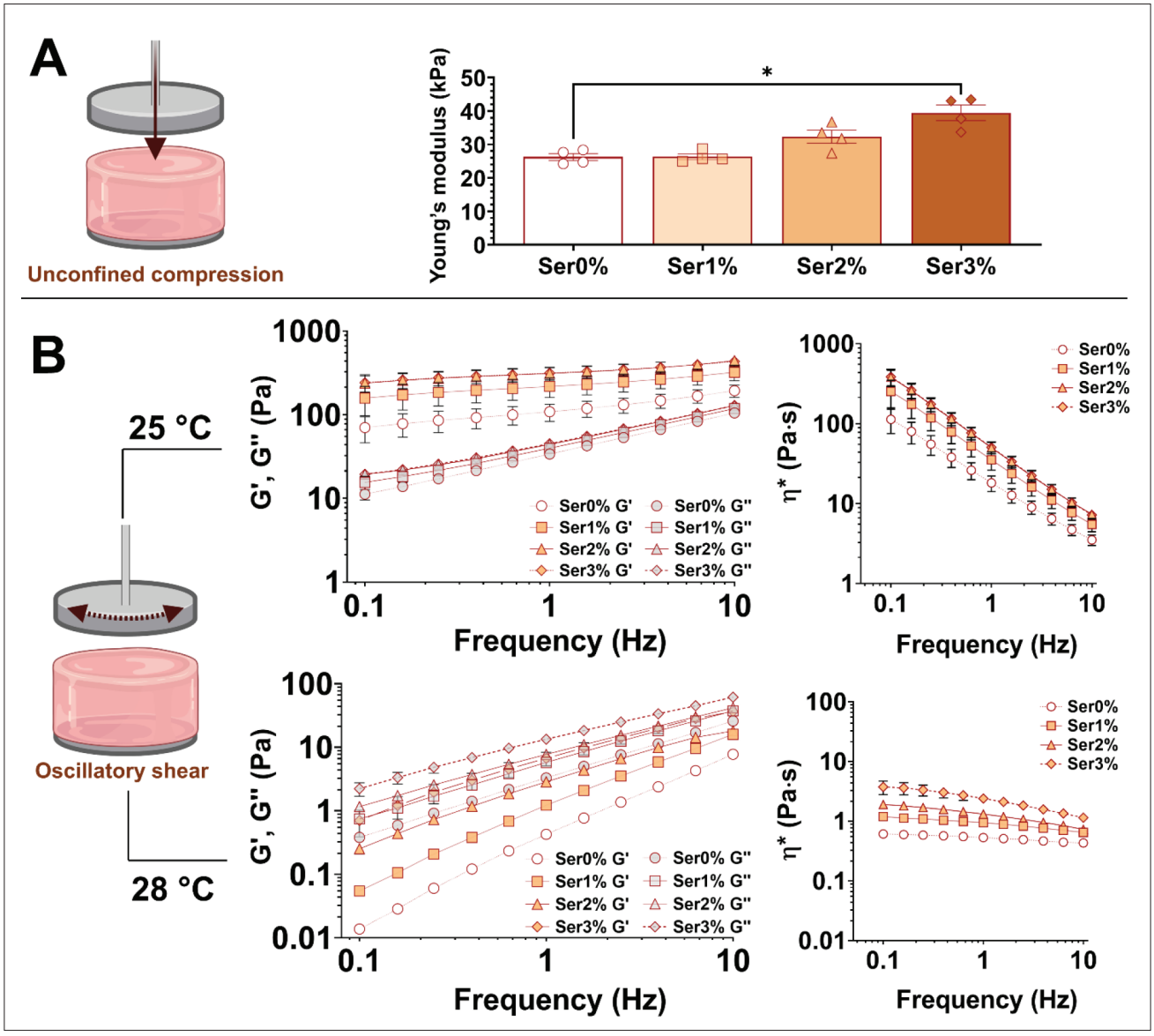

Figure 3. Rheology testing performed on sericin-containing hydrogels. (A) Young's moduli derived from an unconfined compression test. Brown–Forsythe and Welch ANOVA test was used to compare the groups (*$p < 0.05$). (B) Storage moduli (G'), loss moduli (G''), and complex viscosity (η^*) derived from frequency sweep measurements at 25°C (room temperature) and 28°C (printing temperature). Error bars represent the mean ± SE and are within the symbols if not visible ($n = 4$).

mechanical behavior and were previously successfully used by us to characterize the mechanical properties of hydrogels.[29,54,59] Indeed, with rheological analysis, we were able to provide fundamental insights into the materials, including their Young's moduli (Figure 3A) derived from an unconfined compression test, and dynamic moduli (storage modulus G' and loss modulus G'') and complex viscosity (η^*) under oscillatory amplitude sweep testing (Figure 3B). In detail, the addition of sericin to alginate-gelatin hydrogels increased their stiffness, as evidenced by Young's moduli recorded from the unconfined compression test. This effect was directly proportional to the concentration of sericin used and became significant ($p < 0.05$) for Ser3% formulation, which presented the greatest Young's modulus of 39.4 ± 4.7 kPa compared to 26.2 ± 6.4 kPa of Ser0% hydrogel (Figure 3A). Ser1%, Ser2%, and Ser3% improved the ability of Ser0% hydrogel to resist deformation under compressive stress by 4%, 21%, and 50%, respectively. This result was hence confirmed by the oscillatory amplitude sweeps test (Figure 3B). As expected, at a temperature of 25 °C, the storage modulus (G') was predominant on loss modulus (G'') for all biofabricated hydrogels, indicating a solid-like behavior. We detected an increase in the amplitude of the sericin-containing hydrogels' G', compared to Ser0%. This increase was directly proportional to the concentration of protein present, following the Young's moduli recorded (Figure 3A). Likewise, at the same temperature it was noted that as the concentration of sericin increased, the complex viscosity of the hydrogel also increased while preserving the shear thinning behavior of Ser0%. This result was consistent with the increase in BLW magnitude recorded by our Brillouin microspectroscopy analyses (Figure S2, Supporting Information). The same analysis was performed at 28°C to evaluate the hydrogels' mechanical properties during the bioprinting process. The temperature-dependent behavior of alginate-gelatin hydrogel is due to the presence of gelatin. This protein is well known for its thermal-reversible gelation properties, which make its derived mixtures change from *sol-to-gel* according to the temperature (24–30 °C).[60] However, this feature might be changed by the presence of additives, and it depends on the gelatin concentration, molecular weight, and source.[61] Under our experimental conditions, the *gel-to-sol* transition temperature of Ser0% is approximately 28 °C. Therefore, at 25 °C, the temperature is well below the gelation threshold, allowing the formation of a stable gel network and resulting in higher mechanical parameters. In contrast, at 28 °C, the system nears the gelation temperature, leading to partial solubilization and reduced viscoelastic properties. We detected that the gelatin's behavior was not altered by the presence of sericin within the hydrogel network, since at 28 °C, the G'' was larger than G' within the entire frequency range and the viscosity dropped as a function of the frequency amplitude. Despite all hydrogels showing a predominantly liquid-like behavior at 28 °C, for Ser 1%, Ser 2%, and Ser3% hydrogel formulations the proximity between G' and G'' curves is greater with the increase of sericin concentration. This result might indicate that sericin-containing hydrogels retain a greater degree of elasticity than Ser0% formulation. By itself, rheology lacks the micro-scale resolution that Brillouin microspectroscopy analysis provides, thus we further analyzed the biofabricated hydrogels through this contactless approach, based on the process of inelastic scattering that results from light's interaction with thermally excited acoustic phonons in GHz range within the hydrogel structure.[62] This technique allowed us to measure any change in frequency of the light scattered from the sample, known as Brillouin frequency shift (hereafter abbreviated in frequency shift), before and after the crosslinking, and after the incubation with cell culture medium for all formulated hydrogels. Due to the sensitivity of the method, we were able to detect small but significant differences in BFS and BLW magnitudes, which are related to the material's longitudinal elastic modulus and viscosity, respectively.[48,63,64]

Figure 4A demonstrates a significant increase in frequency shift for all sericin-containing hydrogels before crosslinking compared to Ser0% ($p < 0.001$). At this stage, the samples were analyzed after their gelation, and the modifications of frequency shift could be attributed to the change in hydrogels' solid fraction, due to the addition of sericin.[59] As the frequency shift relies both on the polymer concentration and the water content in the sample, we observed a slight reduction in frequency shift values after crosslinking (Figure 4B) and after the incubation with cell culture medium (Figure 4C) since the samples were hydrated by the presence of the crosslinking solution and the medium, respectively. The observed decrease in the frequency shift after crosslinking and incubation in DMEM is consistent with reports in the literature, which emphasize that the water content, rather than the intrinsic stiffness of the material, largely governs the mechanical behavior of hydrogels in physiological conditions.[65] Indeed, after crosslinking, the frequency shift values of both Ser2% and Ser3% hydrogel formulations were significantly changed ($p < 0.001$) compared to the Ser0% ones (Figure 4B), while the addition of sericin at 1% w/v did not alter this property ($p > 0.05$). After we incubated the samples with DMEM (37 °C, 5% CO_2), the increasing trend in frequency shift values with sericin concentration was maintained (Figure 4C), underlying the matrix stiffening effect. The Brillouin frequency shift results were consistent with the

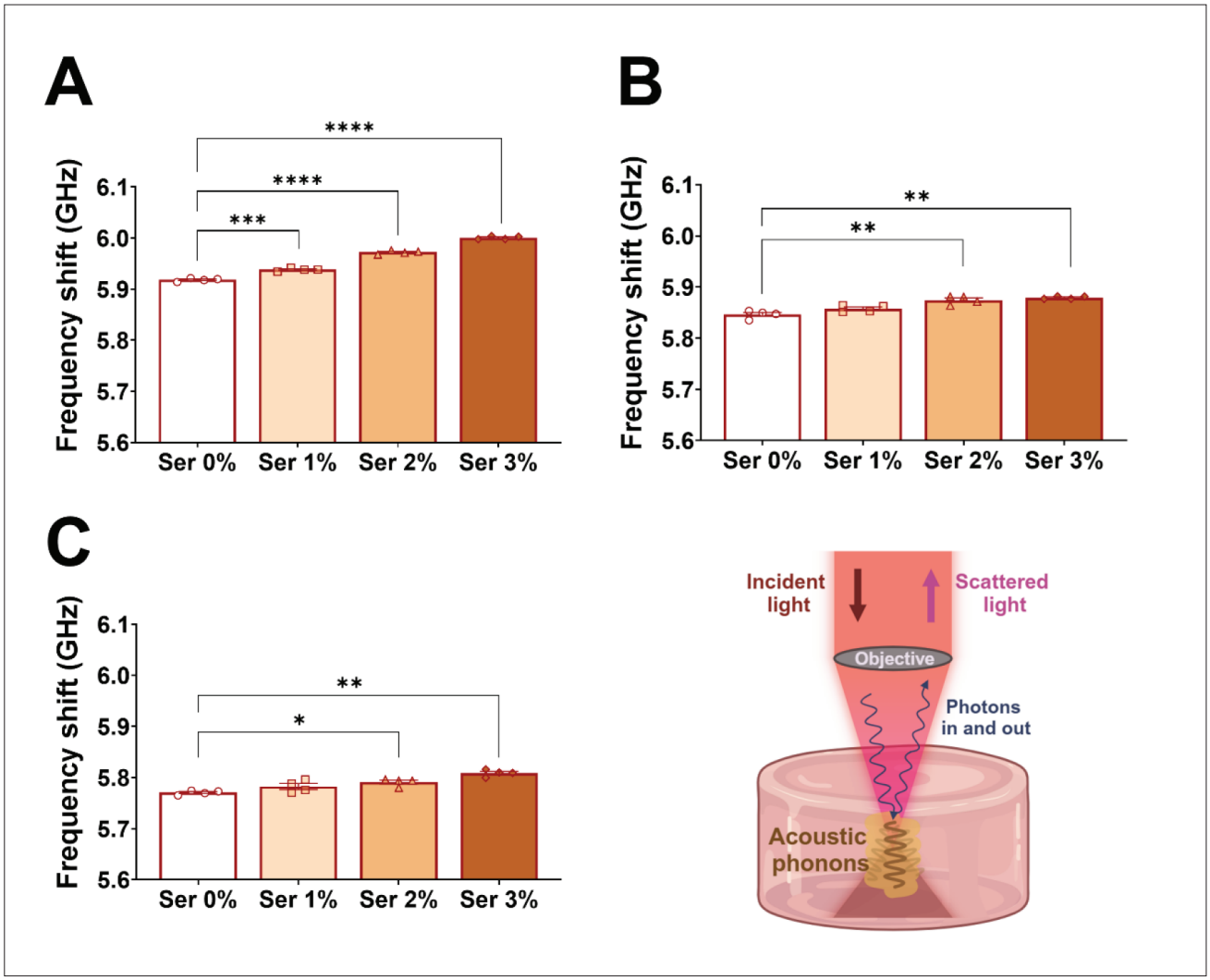

Figure 4. Brillouin microspectroscopy analysis on sericin-containing alginate-gelatin hydrogels. Frequency shift measurements of hydrogels' samples (A) before crosslinking, (B) after cross-linking, and (C) after incubation with the medium. Brown–Forsythe and Welch ANOVA test was used to compare the groups (*$p < 0.05$, **$p < 0.01$, ***$p < 0.001$, **** $p < 0.0001$). Error bars represent the mean ± SE and are within the symbols if not visible ($n = 4$).

ones generated when a different source of sericin was tested (Figure S3, Supporting Information).

Sericin's aminoacidic composition is rich in serine and other polar amino acids, resulting in more carboxyl (—COOH) and hydroxyl (—OH) groups, that may have participated in ionic crosslinking, most likely involving Ca^{2+} ions.[66] This could have facilitated the creation of interpenetrating network hydrogels with increased mechanical strength and therefore increased stiffness. These findings confirmed a greater sensitivity of Brillouin microspectroscopy than classic rheology in understanding mechanical behavior modifications on a microscale and highlighted the contribution of sericin in modulating the mechanical properties of alginate-gelatin hydrogels.

3.2. The addition of sericin increases alginate-gelatin hydrogel porosity

The porosity of a biomaterial plays a major role in biomedical applications since the exchange of nutrients, oxygen, and byproducts depends on the pore size and distribution within the polymeric network, and it is crucial to ensure cells' survival and function.[67] To establish the porosity of the formulated sericin-containing hydrogels, we performed SEM and pore size analysis, together with a gravimetric evaluation of swelling and porosity properties on freeze-dried hydrogel samples. The swelling test revealed an increased ability of sericin-containing hydrogels to absorb aqueous medium compared to the Ser0% formulation, and this effect was directly proportional to the

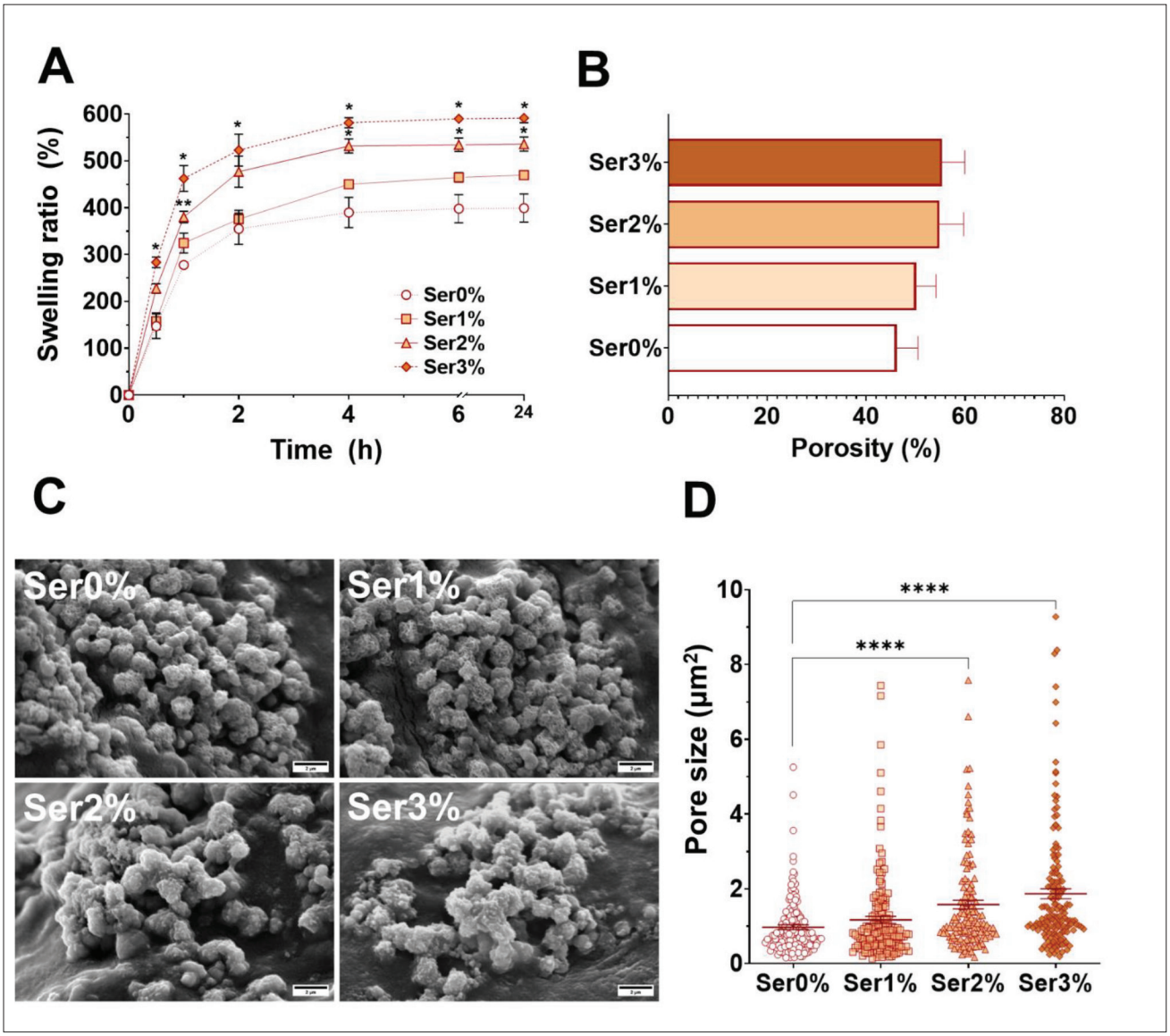

Figure 5. Swelling test, porosity test, and SEM analysis of sericin-containing alginate-gelatin hydrogels. (A) Swelling behavior of sericin-containing hydrogels with two-way ANOVA test with Dunnett's multiple comparisons test as statistical analysis to compare the groups with the control Ser0% (*p <0.05, **p < 0.01; n = 4). (B) Porosity percentages of formulated hydrogel samples after freeze-drying (n = 4). (C) Morphological examination of sericin-containing hydrogel through SEM. Scale bars: 2 μm. (D) Statistical analysis of pore size was performed using Brown–Forsythe and Welch ANOVA test to compare the groups (****p < 0.0001). Error bars represent the mean ± SE and are within the symbols if not visible (n ≥ 15). Abbreviation: SEM, scanning electron microscopy.

increase of sericin concentrations in hydrogels (Figure 5A). Particularly, when compared to the free-sericin hydrogel Ser0%, the swelling ratios were significantly enhanced in Ser2% and Ser3% formulations at almost all evaluated time points (p < 0.05 and p < 0.001, respectively). The maximum swelling equilibrium was reached after 4 h from the beginning of the immersion in PBS, after this time the swelling ratio percentage reached a plateau, independently from the presence of sericin protein within the samples. The presence of sericin could have improved the swelling behavior of alginate-gelatin hydrogels, by increasing the total hydrophilic groups' amount available to attract and interact with water molecules through hydrogen bonding and other polar interactions.[55] Moreover, the improvement of alginate-gelatin swelling properties can be attributed to the increase of the porosity in hydrogel samples with higher sericin concentration, as assessed by the liquid displacement method (Figure 5B). The higher the porosity of the hydrogel, the easier the contact of water molecules with the hydrophilic groups within the polymeric network.[68]

The inner morphology of biofabricated hydrogels was further evaluated by SEM (Figure 5C), and the pore size was measured by calculating the mean inner area of the pores. Based on our statistical analysis (Figure 5D), we found that the inclusion of sericin provided hydrogel networks with larger pores, as a function of the protein content in the hydrogel. In detail, the mean pore size of Ser1%, Ser2%, and Ser3% were increased by 20%, 62%, and 92% compared to the mean pore size of Ser0%. Once again, we recorded the most significant differences ($p < 0.0001$) for the hydrogels containing sericin at concentrations of 2% and 3% w/v. This effect is in positive agreement with previous studies, which reported the same situation for sericin-blends within a certain range of concentration of the protein (2–4% w/v).[67,68]

3.3. Hydrogels containing 3D-bioprinted sericin shows improved printability and durability features

To ascertain any effect related to the addition of sericin to alginate-gelatin hydrogels during the 3D bioprinting process, we carried out printability and durability studies. Once the mechanical and structural characterizations were completed, the biofabricated hydrogels containing increasing concentrations of sericin were bioprinted using the extrusion-based bioprinter BIOX6. We used the same operative parameters for all formulations to assess any difference in the bioprinting process of simple-shaped patches made of two consecutive layers. Although Brillouin microspectroscopy and rheology analyses have proved an increase in elasticity and viscosity as the sericin concentration in hydrogels was increased, all the tested formulations were printable at 28 °C and no occlusion of the nozzle occurred.

We bioprinted at least 12 constructs from each hydrogel formulation (with and without sericin) and assessed the width of each bioprinted strand, which was compared with the inner diameter of the printhead nozzle (0.41 mm) to obtain a ratio of printability. Then, we calculated a normalized printability ratio by comparing the sericin-

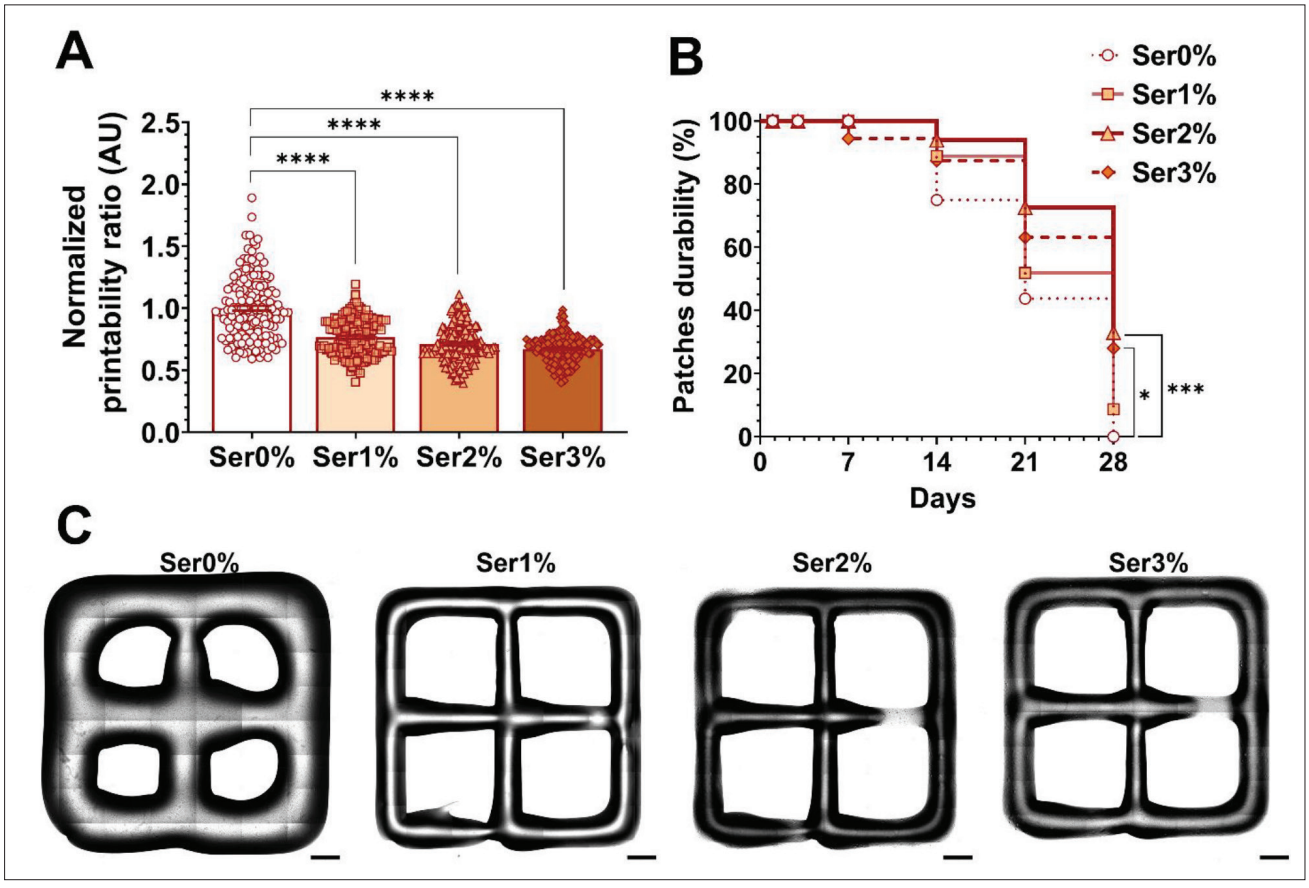

Figure 6. Printability and durability assessments of 3D-bioprinted sericin-containing hydrogels. (A) Statistical analysis of normalized printability ratio of Ser0%, Ser1%, Ser2%, and Ser3% was performed using Brown–Forsythe and Welch ANOVA test to compare the groups (****$p < 0.0001$). Error bars represent the mean ± SE and are within the symbols if not visible ($n = 14$). (B) Statistical analysis of 3D-bioprinted patches durability after crosslinking and incubation with cell culture medium for up to 28 days (37°C, 5% CO2 in air) by using log-rank (Mantel–Cox) test to compare the durability curves (*$p < 0.05$, ***$p < 0.001$, $n \geq 9$). (C) Representative images of 3D-bioprinted patch. Scale bars: 2 mm.

containing hydrogels with our control Ser0% hydrogel. Our statistical analysis showed that the resolution of the patches derived from Ser1%, Ser2%, and Ser3% was significantly improved ($p < 0.0001$) if compared with Ser0% (Figure 6A). This result demonstrated that the addition of sericin caused a reduction of the bioprinted strand widths, which were more similar to the diameter of the nozzle when sericin was included in the hydrogel formulation even at the lowest concentration of 1% w/v, as shown in Figure 6C. This result is in positive agreement with our rheological characterization of sericin-containing hydrogels, which at 28 °C showed greater viscosity values compared to Ser0% (Figure 3B). Previous studies have proved that in extrusion 3D bioprinting, the relationship between the strand diameter and bioink viscosity depends on the bioink shear-thinning or shear-thickening behaviour.[69,70] Our sericin-containing hydrogels all exhibited shear-thinning behaviors (Figure 3B), and in this case, their slightly greater viscosity could have determined a better resolution of the patches concerning the alginate-gelatin hydrogel, without hampering the process.[70]

To establish the durability of the bioprinted structures during a simulated cell culturing condition, we crosslinked the constructs and thus incubated them in the cell culture medium (37 °C, 5% CO_2) for up to 28 days. During this period, the patches were systematically observed through the EVOS M7000 Imaging System to detect any macroscopic and/or microscopic loss of fragments compared to the original structure (an example of the identification of disintegration signs is given in Figure S4, Supporting Infrmation) and to assess their durability, as reported in Figure 6B.

Three days after the beginning of the observation, all the structures maintained their original shape, and we did not record any strand detachment from the main structure, regardless of the presence of sericin. After 14 days, more than 80% of the bioprinted patches from sericin-containing hydrogels maintained their integrity and around 75% of Ser0%-derived patches survived undamaged from the incubation event. At day 28, the wholeness of patches bioprinted from Ser0% hydrogel was disintegrated, whereas the durability of Ser2% and Ser3% patches was statistically different with a 33% ($p < 0.001$) and 28% ($p < 0.05$) of intact structures recorded, respectively. The obtained durability results stated that the addition of sericin at concentrations of 2% and 3% w/v improved the durability of alginate-gelatin hydrogels, while Ser1% did not significantly affect this property (Figure 6B).

Effectively, this effect might be correlated with the increase of hydrogel's elasticity assessed by Brillouin microspectroscopy analysis, which reported a significant increase in the frequency shift for Ser2% and Ser3% compared to Ser0% (Figure 4), even after incubation with cell culture medium. The slight difference between the durability of Ser2%- and Ser3%-derived patches in cell medium could be justified by referring to their swelling behavior (Figure 5A). Indeed, owing to higher swelling rate, Ser3% might have caused slightly more rapid degradation of the bioprinted patches in PBS than Ser2%.[67]

3.4. The addition of sericin improves cardiac cell viability during the first 14 days in culture

To evaluate the effect on cardiac cell viability, we cultured CSs embedded in sericin-containing hydrogels for up to 28 days. CSs encompass the most representative cell types of adult human myocardial tissue, and they can recapitulate the complexity of the cardiac microenvironment.[24] At predetermined timepoints of 3, 14, and 28 days, we performed a live/dead assay. At each time point, the ratio between dead and live cells (henceforth toxicity ratio) was determined by evaluating the fluorescence of calcein-AM and EthD-1. As a cell-permeant dye, calcein-AM can freely diffuse into cells, but its acetoxymethyl ester structure can be cleaved only by intracellular esterase of live cells to produce the related green, fluorescent calcein. On the contrary, EthD-1 can only penetrate cells whose membranes have been damaged thus allowing the dye to bind nucleic acids of dead cells. Figure 7 summarizes the toxicity ratios measured at each time point together with the representative images derived from our confocal analysis. After 3 days, the toxicity ratios of CSs embedded in Ser2% and Ser3% formulations were significantly lower than Ser0% hydrogel. A reduction of 25% ($p < 0.01$) and 26% ($p < 0.001$) of the Ser0% toxicity ratio was recorded for Ser2% and Ser3%, respectively (Figure 7E). This result stated that the sericin concentrations used in hydrogels were not toxic for CSs. Quite the opposite, Ser2% and Ser3% supported the viability of cardiac cells, as stated by the reduction of the toxicity ratio as a result of an increased number of live cells. The observed trend was also confirmed after day 14 (Figure 7J) when we recorded a significant amelioration of the toxicity ratio for both formulations compared to Ser0%. However, after 28 days the toxicity ratio values of CSs embedded in all sericin-containing hydrogels were comparable to Ser0%, without any statistically significant difference (Figure 7O). We speculate that during the first 14 days of culturing in sericin-containing hydrogels, the cardiac cells were able to use the protein as a metabolic source before it was completely depleted, considering the spontaneous degradation of the hydrogel and the partial dissolution of sericin within the cell culture medium (regularly refreshed). This hypothesis is in accordance with

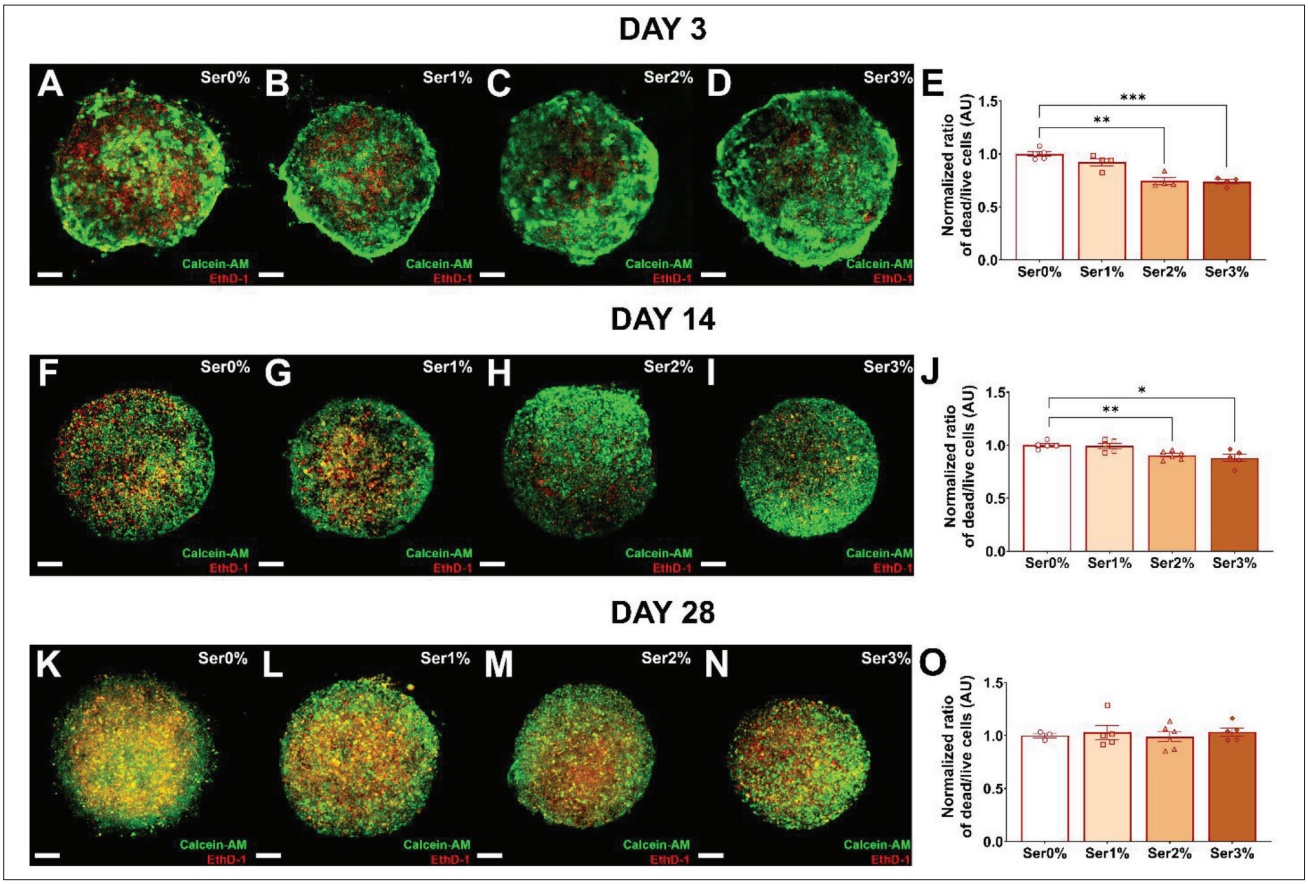

Figure 7. Representative confocal images of Live/Dead assay of CSs embedded in sericin-enriched hydrogels (A–D) after 3 days, (F–I) after 14 days, and (K–N) after 28 days of incubation (37°C, 5% CO2 in air). These images show the live (green, calcein-AM) and dead (red, EthD-1) staining of CSs. Statistical analysis of Dead/Live Cells Ratio of CSs (E) after 3 days, (J) after 14 days, and (O) after 28 days of incubation. Brown–Forsythe and Welch ANOVA test was used to compare the groups (*$p < 0.05$, **$p < 0.01$, ***$p < 0.001$). Error bars represent the mean ± SE and are within the symbols if not visible ($n \geq 3$). Scale bars: 100 μm. Abbreviations: CSs, cardiac spheroids; EthD-1: ethidium homodimer 1.

previous studies demonstrating that sericin enhances cellular energy metabolism and mitochondrial function and reduces apoptosis in cardiomyocytes and endothelial cells.[36,40,41] Sericin's capability to improve the viability and proliferation of certain cell types has been already documented in previous studies and explained as an effect of the protein's naturally cell-adhesive property and ability to affect cellular pathways. For example, the effect of sericin in promoting the viability and migration of human umbilical vessel endothelial cells, as well as antagonizing endothelial cells and cardiomyocytes apoptosis, has been attributed to sericin's intrinsic capability of promoting vascular endothelial growth factor alpha (VEGFα) expression.[36] We reckon that the improved viability of CSs embedded in sericin-containing hydrogels was certainly due to the intrinsic features of the protein, although a great contribution to this effect should be ascribed to the modifications that the protein had on hydrogel properties. Indeed, the reduction of toxicity ratio matched the increase of Ser2% and Ser3% hydrogels' porosity (Figure 5D), together with their improved mechanical properties (Figures 3A and 4C) and enhanced durability (Figure 6B). Moreover, the addition of sericin did not alter the CS contractile activity as demonstrated by the absence of statistically significant differences in both contraction frequency and fractional shortening % (FS%) of CSs embedded in Ser3% compared to the control Ser0% (Figure S5, Supporting Information).

3.5. Sericin-containing hydrogels increase the presence of cardiac fibroblasts in CSs

To evaluate if the addition of sericin could have affected the cell populations of CSs embedded in hydrogels, we performed an immunostaining.[25] Toward this end, after 28 days of culture in the cell medium, the CSs embedded in all formulated hydrogels were labeled to identify HCAECs, HCFs, and iCMs.[29] We thus measured the fluorescence derived from each labeled cell type during the confocal

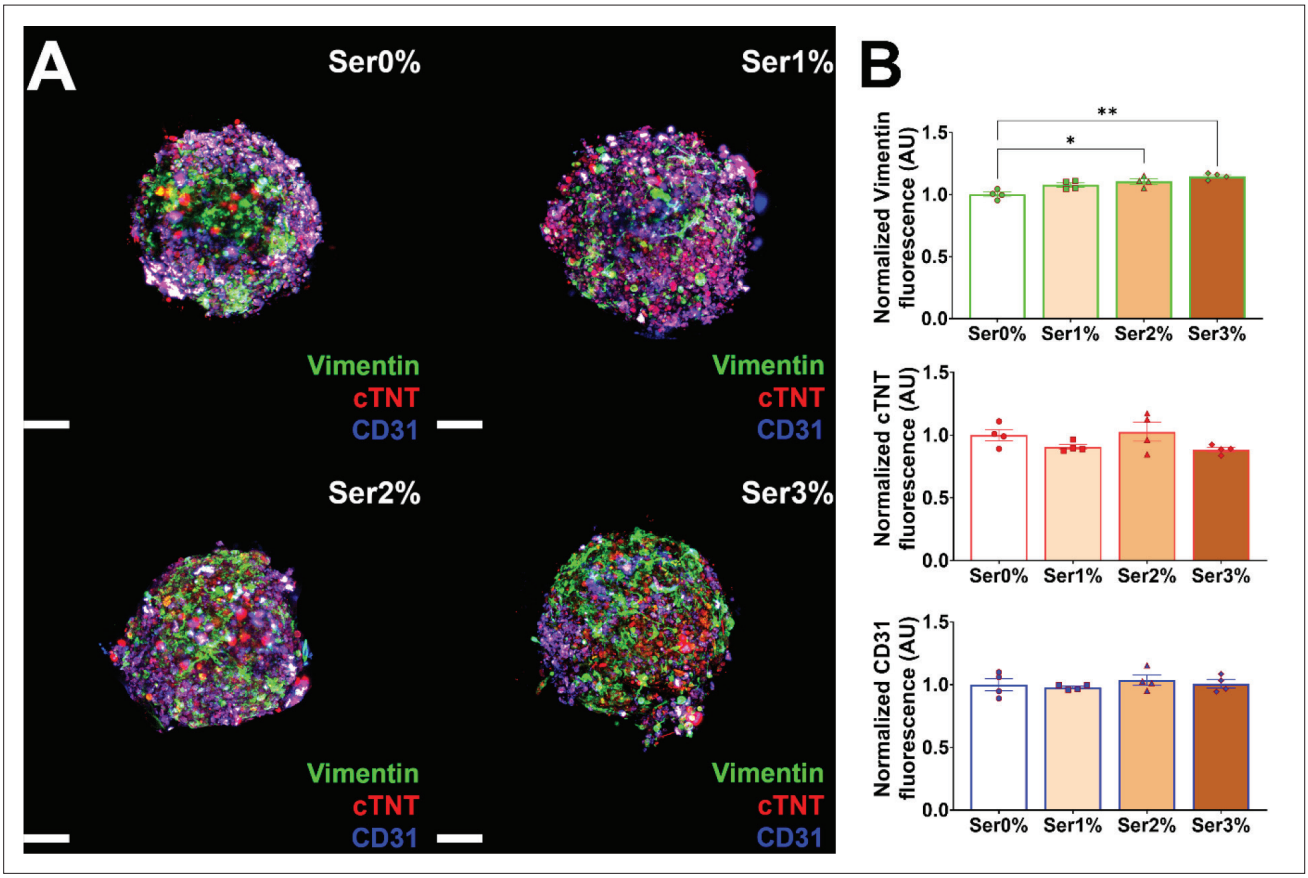

Figure 8. Collapsed z-stacks of confocal images of representative CSs after 28 days of incubation with sericin-containing hydrogels. (A) The CSs were stained with antibodies against vimentin (green) for HCFs, cTNT (red) for iCMs, and CD31 (blue) for HCAECs. Scale bars: 100 µm. (B) Statistical analyses of stained cells fluorescence were performed using Brown–Forsythe and Welch ANOVA test to compare the groups (*p < 0.05, **p < 0.01). Error bars represent the mean ± SE and are within the symbols if not visible (n = 4). Abbreviations: BM, brillouin microspectroscopy; CSs, cardiac spheroids; cTNT, Troponin T-C Antibody (CT3) Alexa Fluor® 546-conjugated; HCAECs, human coronary artery endothelial cells; HCFs, human cardiac fibroblasts; iCMs, iCell® cardiomyocytes.

microscope analysis of samples. Figure 8A shows the collapsed z-stacks of confocal images of representative CSs embedded in both Ser0% and hydrogels with increasing sericin content. Cardiac endothelial cells, fibroblasts, and cardiomyocytes stained with antibodies against CD31 (blue), vimentin (green), and cTNT (red), respectively, were present in all CSs derived from the long-term embedding in Ser1%, Ser2%, and Ser3% as in Ser0%. We did not record a statistically significant reduction of any cell-type fluorescence (Figure 8B). However, we documented an increase in the presence of cardiac fibroblast which was proportional to the protein concentration in hydrogels and became significant for Ser2% ($p < 0.05$) and Ser3% ($p < 0.01$) (Figure 8B). This result was confirmed by the 3D rendering of CSs obtained with Imaris software (Figure 9). The enhanced presence of cardiac fibroblasts after 28 days of embedding in sericin-containing hydrogels is likely related to the increased elasticity properties of Ser2% and Ser3%, justified by both our Brillouin microspectroscopy and rheology studies (Figures 3 and 4). Indeed, fibroblasts are sensitive to mechanical properties such as stiffness and elasticity, and they respond to changes in these parameters by modulating their motility and spreading.[69] For the first time, we documented this effect played on HCFs within CSs generated *in vitro*, since although this property of sericin is not new it has been reported before only for non-cardiac or non-human fibroblasts cell lines.[37,52,54,64,70]

4. Conclusion

In this study, we biofabricated for the first time alginate-gelatin hydrogels supplemented with increasing concentrations of sericin from silkworm *B. mori* and investigated their mechanical and structural properties, together with their potential application in 3D bioprinting as bioinks. Sericin-containing hydrogels exhibited improved

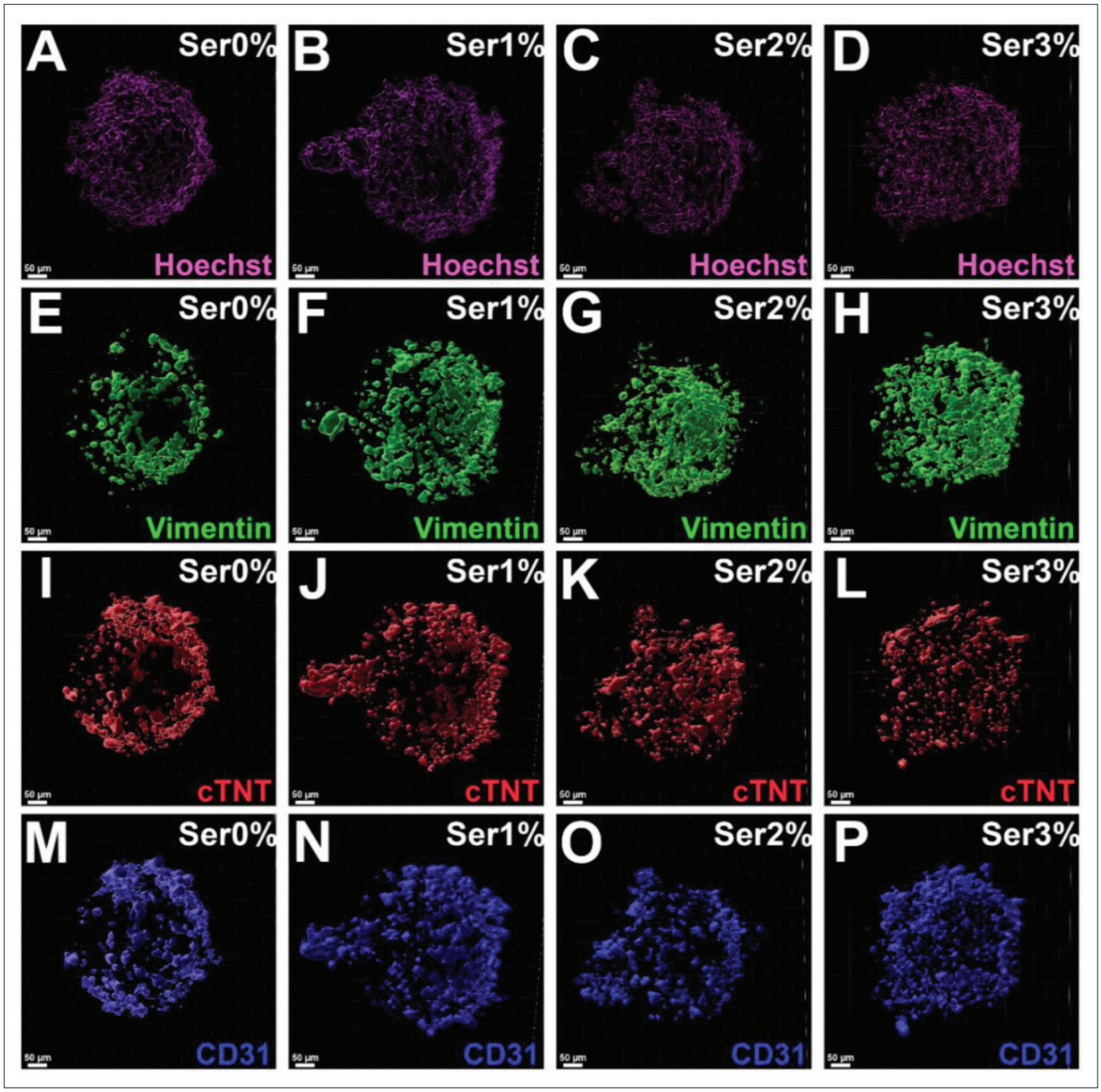

Figure 9. 3D rendering of immunostained CSs after 28 days of culturing in sericin-containing hydrogels. CSs nuclei were stained with (A–D) Hoechst (magenta) and labeled with antibodies against (E–H) vimentin (green, HCFs), (I–L) cTNT (red, iCMs), and (M–P) CD31 (blue, HCAECs). Scale bars: 50 µm. The full-length 3D-rendering videos of CSs are available as Videos S1–S4, Supporting Information..

mechanical properties in terms of elasticity, compression modulus, and viscosity, with higher swelling ratio and enhanced porosity than their counterpart sericin-free hydrogel. These properties ameliorated the performance of alginate-gelatin hydrogel bioink, improving the resolution of 3D-bioprinted patches, as well as their durability during simulated cell culture conditions for up to 28 days. The effects derived from the inclusion of sericin were directly related to its concentration within the polymeric hydrogel network. While Ser1% did not significantly affect alginate-gelatin properties, Ser2% and Ser3% formulations recorded the most significant differences in hydrogel mechanical, morphological, and durability features compared to Ser0%. Also, Ser2% and Ser3% improved CSs viability in hydrogels during the first 2 weeks of culture and Ser3% did not affect the contractile activity of CSs. More interestingly,

sericin-containing hydrogels played an effective role in modulating cardiac fibroblast distribution within CSs, but without altering cardiac endothelial and myocyte cellular populations. These results pave the way for further studies regarding the molecular and mechanotransduction mechanisms underlying these effects. Altogether, our findings support the use of sericin-containing hydrogels as advanced and improved bioinks for cardiac applications. To fully validate the therapeutic potential of these sericin-enriched hydrogels, it will be crucial to examine their adhesive performance and integration within dynamic *in vivo* cardiac environments. Future *in vivo* studies will focus on assessing the therapeutic efficacy, biocompatibility, and potential of sericin-enriched hydrogels in promoting cardiac tissue repair, reducing fibrosis, and enhancing functional recovery following MI.

Acknowledgments

The authors acknowledge the use of the Leica STELLARIS 8 confocal microscope in the Microbial Imaging Facility (MIF) in the Faculty of Science, University of Technology Sydney. They would like to thank Louise Cole and Amy Bottomley for their technical assistance. The authors acknowledge the training and the assistance for SEM analysis provided by Herbert Yuan, Professional Officer in the Microstructural Analysis Unit (MAU) in the Faculty of Science, the University of Technology Sydney.

Funding

Dr. Carmine Gentile was supported by a UTS Seed Funding, Heart Research Australia Grant, Perpetual IMPACT Grant, Catholic Archdiocese of Sydney Grant for Adult Stem Cell Research, and a Heart Research Institute Grant. Irina Kabakova and Hadi Mahmodi are supported by the Australian Research Council Centre of Excellence in Optical Microcombs for Breakthrough Science (CE230100006) and the Australian Research Council Centre of Excellence in Quantum Biotechnology (CE230100021). Thomas R. Cox is supported by the National Health and Medical Research Council (NHMRC). Kaitlin Wyllie is supported by the University Postgraduate Award (UPA) from the University of New South Wales (UNSW). Donatella Paolino was supported by grants from the Italian Ministry of Health (PSC SALUTE 2014–2020-POS4 "Cal-Hub-Ria"-T4-AN-09), and PNRR MAD-2022-12376814).

Conflict of interest

Carmine Gentile serves as the Guest Editor of the special issue: *3D Bioprinting DownUnder: Innovation, Advancements and Perspectives*, but did not in any way involve in the editorial and peer-review process conducted for this paper, directly or indirectly. Separately, other authors declare they have no competing interests.

Author contributions

Conceptualization: Carmine Gentile, Martine Tarsitano, Irina Kabakova, Thomas R. Cox, Donatella Paolino
Investigation: Martine Tarsitano, Clara Liu Chung Ming, Dana Idais, Hadi Mahmodi
Methodology: Martine Tarsitano, Carmine Gentile
Validation: Carmine Gentile, Irina Kabakova, Thomas R. Cox
Resources: Benedetta Isella, Carmine Gentile
Data Curation: Martine Tarsitano, Clara Liu Chung Ming, Kaitlin Wyllie
Visualization: Martine Tarsitano, Carmine Gentile
Supervision: Carmine Gentile, Donatella Paolino
Formal analysis: Carmine Gentile, Hadi Mahmodi
Writing – original draft: Martine Tarsitano
Writing – review & editing: Martine Tarsitano, Carmine Gentile, Irina Kabakova, Thomas R. Cox, Donatella Paolino
All authors have read and agreed to the published version of the manuscript.

Ethics approval and consent to participate

Not applicable.

Consent for publication

Not applicable.

Availability of data

Data is available from the corresponding author upon reasonable request.

Further disclosure

Part of or the entire set of findings have been presented in the 2024 Australian Bioprinting Workshop for Tissue Engineering and Regenerative Medicine (Sydney).

References

1. Tsao CW, Aday AW, Almarzooq ZI, et al. Heart disease and stroke statistics—2023 update: a report from the American Heart Association. *Circulation*. 2023;147(8):e93-e621. doi: 10.1161/CIR.0000000000001123

2. Cooke JP. Is cardiovascular regeneration possible? *Methodist Debakey Cardiovasc J*. 2023;19(5):1-4. doi: 10.14797/mdcvj.1307

3. Frantz S, Hundertmark MJ, Schulz-Menger J, Bengel FM, Bauersachs J. Left ventricular remodelling post-myocardial infarction: pathophysiology, imaging, and novel therapies. *Eur Heart J.* 2022;43(27):2549-2561. doi: 10.1093/eurheartj/ehac223

4. Schwinger RHG. Pathophysiology of heart failure. *Cardiovasc Diagn Ther.* 2021;11(1):263-276. doi: 10.21037/cdt-20-302

5. Awad MA, Shah A, Griffith BP. Current status and outcomes in heart transplantation: a narrative review. *Rev Cardiovasc Med.* 2022;23(1):11. doi: 10.31083/j.rcm2301011

6. Mantha A, Lee RO, Jr., Wolfson AM. Patient selection for heart transplant: balancing risk. *Curr Opin Organ Transplant.* 2022;27(1):36-44. doi: 10.1097/mot.0000000000000943

7. Benck L, Kransdorf EP, Emerson DA, et al. Recipient and surgical factors trigger severe primary graft dysfunction after heart transplant. *J Heart Lung Transplant.* 2021;40(9):970-980. doi: 10.1016/j.healun.2021.06.002

8. Huang K, Ozpinar EW, Su T, et al. An off-the-shelf artificial cardiac patch improves cardiac repair after myocardial infarction in rats and pigs. *Sci Transl Med.* 2020;12(538):eaat9683. doi: 10.1126/scitranslmed.aat9683

9. Wu CA, Zhu Y, Woo YJ. Advances in 3D bioprinting: techniques, applications, and future directions for cardiac tissue engineering. *Bioengineering (Basel).* 2023; 10(7):842. doi: 10.3390/bioengineering10070842

10. Das S, Nam H, Jang J. 3D bioprinting of stem cell-laden cardiac patch: a promising alternative for myocardial repair. *APL Bioeng.* 2021;5(3):031508. doi: 10.1063/5.0030353

11. Budharaju H, Sundaramurthi D, Sethuraman S. Efficient dual crosslinking of protein-in-polysaccharide bioink for biofabrication of cardiac tissue constructs. *Biomater Adv.* 2023;152:213486. doi: 10.1016/j.bioadv.2023.213486

12. Zheng Z, Tang W, Li Y, et al. Advancing cardiac regeneration through 3D bioprinting: methods, applications, and future directions. *Heart Fail Rev*. 2024;29(3):599-613. doi: 10.1007/s10741-023-10367-6

13. Yao Y, Li A, Wang S, et al. Multifunctional elastomer cardiac patches for preventing left ventricle remodeling after myocardial infarction in vivo. *Biomaterials*. 2022;282: 121382. doi: 10.1016/j.biomaterials.2022.121382

14. Garbern JC, Lee RT. Heart regeneration: 20 years of progress and renewed optimism. *Dev Cell.* 2022;57(4):424-439. doi: 10.1016/j.devcel.2022.01.012

15. Liu Chung Ming C, Ben-Sefer E, Gentile C. Stem cell-based 3D bioprinting for cardiovascular tissue regeneration. In: Zhang J, Serpooshan V, eds. *Advanced Technologies in Cardiovascular Bioengineering*. Springer International Publishing; 2022:281-312. doi: 10.1007/978-3-030-86140-7_13

16. Brazhkina O, Park JH, Park HJ, et al. Designing a 3D printing based auxetic cardiac patch with hiPSC-CMs for heart repair. *J Cardiovasc Dev Dis.* 2021;8(12):172. doi: 10.3390/jcdd8120172

17. Matthews N, Pandolfo B, Moses D, Gentile C. Taking it personally: 3D bioprinting a patient-specific cardiac patch for the treatment of heart failure. *Bioengineering.* 2022;9(3):93. doi: 10.3390/bioengineering9030093

18. Budharaju H, Subramanian A, Sethuraman S. Recent advancements in cardiovascular bioprinting and bioprinted cardiac constructs. *Biomater Sci.* 2021;9(6):1974-1994. doi: 10.1039/D0BM01428A

19. Lu TY, Xiang Y, Tang M, Chen S. 3D printing approaches to engineer cardiac tissue. *Curr Cardiol Rep.* 2023;25(6):505-514. doi: 10.1007/s11886-023-01881-y

20. Baheiraei N, Razavi M, Ghahremanzadeh R. Reduced graphene oxide coated alginate scaffolds: potential for cardiac patch application. *Biomater Res.* 2023; 27(1):109. doi: 10.1186/s40824-023-00449-9

21. Fischer B, Gwinner F, Gepp MM, et al. A highly versatile biopolymer-based platform for the maturation of human pluripotent stem cell-derived cardiomyocytes enables functional analysis in vitro and 3D printing of heart patches. *J Biomed Mater Res A.* 2023;111(10):1600-1615. doi: 10.1002/jbm.a.37558

22. Loureiro J, Miguel SP, Galván-Chacón V, et al. Three-dimensionally printed hydrogel cardiac patch for infarct regeneration based on natural polysaccharides. *Polymers.* 2023;15(13):2824. doi: 10.3390/polym15132824

23. Kazemi Asl S, Rahimzadegan M, Ostadrahimi R. The recent advancement in the chitosan hybrid-based scaffolds for cardiac regeneration after myocardial infarction. *Carbohydr Polym.* 2023;300:120266. doi: 10.1016/j.carbpol.2022.120266

24. Sharma P, Gentile C. Cardiac spheroids as in vitro bioengineered heart tissues to study human heart pathophysiology. *J Vis Exp.* 2021;167(167):33554972. doi: 10.3791/61962

25. Polonchuk L, Chabria M, Badi L, et al. Cardiac spheroids as promising in vitro models to study the human heart microenvironment. *Sci Rep*. 2017;7(1):7005. doi: 10.1038/s41598-017-06385-8

26. Sharma P, Liu Chung Ming C, Wang X, et al. Biofabrication of advanced in vitro 3D models to study ischaemic and doxorubicin-induced myocardial damage. *Biofabrication*. 2022;14(2):109-116.
doi: 10.1088/1758-5090/ac47d8

27. Sharma P, Wang X, Ming CLC, et al. Considerations for the bioengineering of advanced cardiac in vitro models of myocardial infarction. *Small*. 2021;17(15):e2003765.
doi: 10.1002/smll.202003765

28. Roche CD, Lin H, Huang Y, et al. 3D bioprinted alginate-gelatin hydrogel patches containing cardiac spheroids recover heart function in a mouse model of myocardial infarction. *Bioprinting*. 2023;30:e00263.
doi: 10.1016/j.bprint.2023.e00263

29. Polonchuk L, Surija L, Lee MH, et al. Towards engineering heart tissues from bioprinted cardiac spheroids. *Biofabrication*. 2021;13(4):34265755.
doi: 10.1088/1758-5090/ac14ca

30. Roche CD, Sharma P, Ashton AW, Jackson C, Xue M, Gentile C. Printability, durability, contractility and vascular network formation in 3D bioprinted cardiac endothelial cells using alginate-gelatin hydrogels. *Front Bioeng Biotechnol*. 2021;9:636257.
doi: 10.3389/fbioe.2021.636257

31. Saad M, El-Samad LM, Gomaa RA, Augustyniak M, Hassan MA. A comprehensive review of recent advances in silk sericin: extraction approaches, structure, biochemical characterization, and biomedical applications. *Int J Biol Macromol* 2023;250:126067.
doi: 10.1016/j.ijbiomac.2023.126067

32. Sahoo JK, Hasturk O, Falcucci T, Kaplan DL. Silk chemistry and biomedical material designs. *Nat Rev Chem*. 2023;7(5):302-318.
doi: 10.1038/s41570-023-00486-x

33. Liu J, Shi L, Deng Y, et al. Silk sericin-based materials for biomedical applications. *Biomaterials*. 2022;287:121638.
doi: 10.1016/j.biomaterials.2022.121638

34. Capar G, Pilevneli T. Cost-effective process development for sericin recovery from silk degumming wastewater. *Sustain Chem Pharm*. 2024;37:101405.
doi: 10.1016/j.scp.2023.101405

35. Silva AS, Costa EC, Reis S, et al. Silk sericin: a promising sustainable biomaterial for biomedical and pharmaceutical applications. *Polymers*. 2022;14(22):4931.
doi: 10.3390/polym14224931

36. Song Y, Zhang C, Zhang J, et al. An injectable silk sericin hydrogel promotes cardiac functional recovery after ischemic myocardial infarction. *Acta Biomater*. 2016;41:210-223.
doi: 10.1016/j.actbio.2016.05.039

37. Han L, Wang W, Chen Z, et al. Sericin-reinforced dual-crosslinked hydrogel for cartilage defect repair. *Colloids Surf B Biointerfaces*. 2023;222:113061.
doi: 10.1016/j.colsurfb.2022.113061

38. Zhang Y, Liu J, Huang L, Wang Z, Wang L. Design and performance of a sericin-alginate interpenetrating network hydrogel for cell and drug delivery. *Sci Rep*. 2015;5:12374.
doi: 10.1038/srep12374

39. Li Y, Wei Y, Zhang G, Zhang Y. Sericin from fibroin-deficient silkworms served as a promising resource for biomedicine. *Polymers*. 2023;15(13):2941.
doi: 10.3390/polym15132941

40. Rahimpour S, Jabbari H, Yousofi H, et al. Regulatory effect of sericin protein in inflammatory pathways; a comprehensive review. *Pathol Res Pract*. 2023;243:154369.
doi: 10.1016/j.prp.2023.154369

41. Rujimongkon K, Ampawong S, Isarangkul D, Reamtong O, Aramwit P. Sericin-mediated improvement of dysmorphic cardiac mitochondria from hypercholesterolaemia is associated with maintaining mitochondrial dynamics, energy production, and mitochondrial structure. *Pharm Biol*. 2022;60(1):708-721.
doi: 10.1080/13880209.2022.2055088

42. Zhu Y, Liu H, Qin S, et al. Antibacterial sericin cryogels promote hemostasis by facilitating the activation of coagulation pathway and platelets. *Adv Healthc Mater*. 2022;11(11):2102717.
doi: 10.1002/adhm.202102717

43. Mukherjee S, Krishnan A, Athira RK, Kasoju N, Sah MK. Chapter 13 - silk fibroin and silk sericin in skin tissue engineering and wound healing: retrospect and prospects. In: Sah MK, Kasoju N, Mano JF, eds. *Natural Polymers in Wound Healing and Repair*. Elsevier; 2022: 301-331.
doi: 10.1016/B978-0-323-90514-5.00005-5

44. Vettori L, Sharma P, Rnjak-Kovacina J, Gentile C. 3D bioprinting of cardiovascular tissues for in vivo and in vitro applications using hybrid hydrogels containing silk fibroin: state of the art and challenges. *Curr Tissue Microenviron Rep*. 2020;1(4):261-276.
doi: 10.1007/s43152-020-00026-5

45. Song Y, Wang H, Yue F, et al. Silk-based biomaterials for cardiac tissue engineering. *Adv Healthc Mater*. 2020;9(23):e2000735.
doi: 10.1002/adhm.202000735

46. Tarsitano M, Mancuso A, Cristiano MC, Paolino D, Fresta M. In situ swelling formulation of glycerol-monooleate-derived lyotropic liquid crystals proposed for local vaginal application. *Molecules*. 2022;27(19):6295.
doi: 10.3390/molecules27196295

47. Mancuso A, Cianflone E, Cristiano MC, et al. Lyotropic liquid crystals: a biocompatible and safe material for local cardiac application. *Pharmaceutics*. 2022;14(2):452.
doi: 10.3390/pharmaceutics14020452

48. Mahmodi H, Piloni A, Utama RH, Kabakova I. Mechanical mapping of bioprinted hydrogel models by brillouin microscopy. *Bioprinting*. 2021;23:e00151. doi: 10.1016/j.bprint.2021.e00151

49. Baptista M, Joukhdar H, Alcala-Orozco CR, et al. Silk fibroin photo-lyogels containing microchannels as a biomaterial platform for in situ tissue engineering. *Biomater Sci*. 2020;8(24):7093-7105. doi: 10.1039/d0bm01010c

50. Schneider CA, Rasband WS, Eliceiri KW. NIH Image to ImageJ: 25 years of image analysis. *Nat Methods*. 2012;9(7):671-675. doi: 10.1038/nmeth.2089

51. Tarsitano M, Liu Chung Ming C, Bennar L, et al. Chlorella-enriched hydrogels protect against myocardial damage and reactive oxygen species production in an in vitro ischemia/reperfusion model using cardiac spheroids. *Biofabrication*. 2025;17(1):015006. doi: 10.1088/1758-5090/ad8266

52. Zhang Y, Cao X, Zhang J, et al. A novel injectable sericin hydrogel with strong fluorescence for tracing. *Int J Biol Macromol*. 2024;258:129000. doi: 10.1016/j.ijbiomac.2023.129000

53. Li J-X, Zhao S-X, Zhang Y-Q. Silk protein composite bioinks and their 3D scaffolds and in vitro characterization. *Int J Mol Sci*. 2022;23(2):910. doi: 10.3390/ijms23020910

54. Vettori L, Tran HA, Mahmodi H, et al. Silk fibroin increases the elasticity of alginate-gelatin hydrogels and regulates cardiac cell contractile function in cardiac bioinks. *Biofabrication*. 2024;16(3):035025. doi: 10.1088/1758-5090/ad4f1b

55. Baptista-Silva S, Borges S, Costa-Pinto AR, et al. In situ forming silk sericin-based hydrogel: a novel wound healing biomaterial. *ACS Biomater Sci Eng*. 2021;7(4):1573-1586. doi: 10.1021/acsbiomaterials.0c01745

56. Chlapanidas T, Faragò S, Lucconi G, et al. Sericins exhibit ROS-scavenging, anti-tyrosinase, anti-elastase, and in vitro immunomodulatory activities. *Int J Biol Macromol*. 2013;58:47-56. doi: 10.1016/j.ijbiomac.2013.03.054

57. Rocha LK, Favaro LI, Rios AC, et al. Sericin from Bombyx mori cocoons. Part I: extraction and physicochemical-biological characterization for biopharmaceutical applications. *Process Biochem*. 2017;61:163-177. doi: 10.1016/j.procbio.2017.06.019

58. Sellimi S, Younes I, Ayed HB, et al. Structural, physicochemical and antioxidant properties of sodium alginate isolated from a Tunisian brown seaweed. *Int J Biol Macromol*. 2015;72:1358-1367. doi: 10.1016/j.ijbiomac.2014.10.016

59. Rad MA, Mahmodi H, Filipe EC, Cox TR, Kabakova I, Tipper JL. Micromechanical characterisation of 3D bioprinted neural cell models using Brillouin microspectroscopy. *Bioprinting*. 2022;25:e00179. doi: 10.1016/j.bprint.2021.e00179

60. Avallone PR, Romano M, Sarrica A, Delmonte M, Pasquino R, Grizzuti N. Effect of sugars on gelation kinetics of gelatin gels. *Fluids*. 2022;7(5):163. doi: 10.3390/fluids7050163

61. Ahmad MI, Li Y, Pan J, et al. Collagen and gelatin: structure, properties, and applications in food industry. *Int J Biol Macromol*. 2024;254:128037. doi: 10.1016/j.ijbiomac.2023.128037

62. Poon C, Chou J, Cortie M, Kabakova I. Brillouin imaging for studies of micromechanics in biology and biomedicine: from current state-of-the-art to future clinical translation. *J Phys Photonics*. 2021;3(1):012002. doi: 10.1088/2515-7647/abbf8c

63. Rioboó RJJ, Gontán N, Sanderson D, Desco M, Gómez-Gaviro MV. Brillouin spectroscopy: from biomedical research to new generation pathology diagnosis. *Int J Mol Sci*. 2021;22(15):8055. doi: 10.3390/ijms22158055

64. Kabakova I, Zhang J, Xiang Y, et al. Brillouin microscopy. *Nature Revs Methods Primers*. 2024;4(1):8. doi: 10.1038/s43586-023-00286-z

65. Wu P-J, Kabakova IV, Ruberti JW, et al. Water content, not stiffness, dominates Brillouin spectroscopy measurements in hydrated materials. *Nat Methods*. 2018;15(8):561-562. doi: 10.1038/s41592-018-0076-1

66. Tao G, Cai R, Wang Y, Zuo H, He H. Fabrication of antibacterial sericin based hydrogel as an injectable and mouldable wound dressing. *Mater Sci Eng C*. 2021;119:111597. doi: 10.1016/j.msec.2020.111597

67. Ekasurya W, Sebastian J, Puspitasari D, Asri PPP, Asri LATW. Synthesis and degradation properties of Sericin/PVA hydrogels. *Gels*. 2023;9(2):76. doi: 10.3390/gels9020076

68. Zhang Y, Chen H, Li Y, et al. A transparent sericin-polyacrylamide interpenetrating network hydrogel as visualized dressing material. *Polymer Test*. 2020;87:106517. doi: 10.1016/j.polymertesting.2020.106517

69. Miri AK, Mirzaee I, Hassan S, et al. Effective bioprinting resolution in tissue model fabrication. *Lab Chip*. 2019;19(11):2019-2037. doi: 10.1039/C8LC01037D

70. Schwartz R, Malpica M, Thompson GL, Miri AK. Cell encapsulation in gelatin bioink impairs 3D bioprinting resolution. *J Mech Behav Biomed Mater*. 2020;103:103524. doi: 10.1016/j.jmbbm.2019.103524